Technical Report
TR-19-17
March 2020

Transient simulations of the Eurasian ice sheet during the Saalian glacial cycle

Florence Colleoni
Johan Liakka

SVENSK KÄRNBRÄNSLEHANTERING AB

SWEDISH NUCLEAR FUEL
AND WASTE MANAGEMENT CO

Box 3091, SE-169 03 Solna
Phone +46 8 459 84 00
skb.se

SVENSK KÄRNBRÄNSLEHANTERING

ISSN 1404-0344
SKB TR-19-17
ID 1885414
March 2020

Transient simulations of the Eurasian ice sheet during the Saalian glacial cycle

Florence Colleoni, Istituto Nazionale di Oceanografia e Geofisica Sperimentale

Johan Liakka, Svensk Kärnbränslehantering AB

Keywords: Penultimate glacial cycle, Late Saalian, Transient simulations, Ice-sheet.

A pdf version of this document can be downloaded from www.skb.se.

© 2020 Svensk Kärnbränslehantering AB

Preface

This report describes a study on the transient behaviour of the Eurasian ice sheet during the penultimate, Saalian, glaciation (from ~ 241 to 135 thousands of years before present). This constitutes the glaciation with the largest known Eurasian ice sheet of the Quaternary period. Transient thermo-mechanical ice-sheet model simulations for this period were forced by climate modelling output and information on past climate variability from geological archives. The resulting ice-sheet reconstructions are planned to be used as input to bedrock stress modelling carried out for the assessment of long-term safety for spent nuclear fuel repositories at Forsmark, Sweden, and Olkiluoto, Finland.

The study was conducted by Florence Colleoni (Istituto Nazionale di Oceanografia e Geofisica Sperimentale, Trieste, Italy) and Johan Liakka (SKB).

The report manuscript was scientifically reviewed by Prof. Ralf Greve (Glacier and Ice Sheet Research Institute of Low Temperature Science Hokkaido University, Japan). Input to an earlier version of the manuscript was provided by Jens-Ove Näslund (SKB) and Christina Truedsson (Tintra consult).

Stockholm, March 2020

Jens-Ove Näslund
Coordinator Climate Research Programme SKB

Abstract

In this report, a numerical thermomechanical ice-sheet model is used to reconstruct exemplified transient evolutions of the Eurasian ice sheet during the penultimate, Saalian, glacial cycle ~ 241 to 135 thousands of years before present (ka BP). This constitutes the period with the largest Eurasian ice sheet interpreted from Quaternary geological records (approximately the last 2.6 Ma). The numerical ice-sheet reconstructions are planned to be used as input to bedrock stress modelling carried out for the assessment of long-term safety for spent nuclear fuel repositories at Forsmark, Sweden, and Olkiluoto, Finland. To that end, the objective of this study is not to provide the most realistic geographical ice-sheet distribution at every stage of the Saalian glacial cycle. Such a task would indeed be difficult to complete due to the lack of reliable climate data for the Saalian period. Instead, the aim of the present study is to provide temporal ice sheet reconstructions that are in broad agreement with some of the main structural features seen in the data, i.e: (i) a temporal global ice volume evolution broadly in line with geological data of the last 800 ka with a relatively slow ice-sheet build-up followed by a rapid deglaciation; (ii) a simulated global-ice volume during the Late Saalian glacial maximum (~ 140 ka BP) in reasonable agreement with contemporary sea-level reconstructions; and (iii) a significantly larger maximum ice-sheet thickness compared to the corresponding thickness in SKB's reconstruction of the last glacial cycle, the Weichselian.

The transient design of the simulations implied that the ice sheets needed to be forced by a time-dependent representation of surface air temperature, precipitation, sea level and sub-ice shelf ocean melt rates. The climate forcing was first constructed by using results from three equilibrium simulations carried out with a fully-coupled Atmosphere Ocean General Circulation Model (AOGCM). These equilibrium climate simulations are representative for the beginning of the Saalian glacial cycle (239 ka BP), the Saalian glacial maximum (140 ka BP) and the end of the glacial cycle (i.e. the Eemian interglacial at around 125 ka BP). The temporal climate evolution for the time periods between the equilibrium simulations was inferred from geological records. These records were then used to construct so-called climate indices that describe the temporal evolution of the climate through the entire Saalian glacial cycle.

Two control simulations were carried out with the ice-sheet model at 40 km and 100 km horizontal resolution. In the simulation using 100 km resolution, the ice-sheet thickness reached a maximum value of ~ 3 800 m in the Forsmark area and ~ 3 900 m in the Olkiluoto area after about 110 ka into the glacial cycle. Thereafter, most of the Northern Hemisphere ice sheets, including the Eurasian one, decayed in only ~ 10 000 years. Using the 40 km resolution control simulation, the ice cover over Forsmark and Olkiluoto became approximately 200 and 100 m thicker than in the 100 km resolution runs, respectively.

In addition to the control simulations, a number of sensitivity simulations were carried out in order to assess the impact on the transient ice-sheet evolution of climate indices, atmospheric lapse rate representation, surface mass balance related parameters, and formulation of calving and sub-shelf melting. Out of those features, the transient ice-sheet evolution was only found to be sensitive to the chosen climate index, both in regards to Northern Hemisphere ice-volume evolution and ice-sheet thickness over the two repository sites. In total, four different climate indices were used, based on different geological archives. Of those four indices, only two managed to simulate a Saalian ice cover over Forsmark and Olkiluoto, whereas the other two failed to simulate an ice cover over the sites. The widely different responses of the ice-sheet evolution to the employed climate indices illustrate the large uncertainty related to the transient climate evolution during the Saalian glacial cycle.

A peculiarity of virtually all simulations conducted here is that they developed a large East Siberian ice sheet connected to the Eurasian and North American ice sheets. The existence of such an ice sheet during the Saalian glacial cycle is supported by recent studies but remains highly debated. In order to not have the results over Eurasia affected by this uncertain ice configuration, the physical connection between the East Siberian and both the North American and Eurasian ice sheets was inhibited by imposing an artificial narrow high surface air temperature corridor between the Siberian ice cap and adjacent North American and Eurasian ice sheets.

Despite the limitations discussed above, the simulations presented here exhibit a reasonable transient development of the Saalian glacial cycle, characterised by a relatively slow ice-sheet build-up followed by a faster decay, and a maximum Eurasian ice-sheet extent that is in general agreement with geological data. In addition, the simulations provided in this study result in a considerably thicker (~ 1 000 m) Eurasian ice sheet than in reconstructions of the Weichselian ice sheet, and are therefore considered suitable for studying the transient impact of extreme glaciation on the bedrock stress distributions in Fennoscandia.

Sammanfattning

I denna studie används en numerisk termomekanisk inlandsismodell för att rekonstruera exemplifierande transienta utvecklingar hos den euroasiatiska isen under den näst senaste glaciala cykeln (Saaleglaciationen) mellan ~ 241 000 och 135 000 år före nutid. Denna glaciala period karakteriseras av att den hade den största eurasiska inlandsis som har identifierats i kvartärgeologiska arkiv. De numeriska inlandsisrekonstruktionerna kommer att användas som randvillkor för modellering av spänningsfältet i berggrunden. Denna modellering ingår i sin tur i analyserna av långsiktig säkerhet för de planerade kärnbränsleförvaren i Forsmark, Sverige och Olkiluoto, Finland. I spänningsanalysen kommer Saaleglaciationen att utgöra ett gränssättande fall för mäktigast inlandsis. Mot bakgrund av detta är målet med studien inte att ta fram en fulländad inlandsisutveckling för Saaleglaciationen, vilket dessutom skulle vara mycket svårt på grund av bristen på tillförlitlig data som beskriver klimatutvecklingen under Saale. Målet är istället att ta fram en tidsberoende inlandsisrekonstruktion som till rimlig grad uppvisar distinkta kännetecken hos Saaleglaciationen, nämligen: i) att tidsutvecklingen hos den globala isvolymen ska stämma överens med den generella bilden av glaciala cykler under de senaste 800 000 åren, dvs med en relativt långsam uppbyggnad av inlandsis följd av en snabb deglaciation; ii) den simulerade globala isvolymen vid Saaleglaciationens maximum (cirka 140 000 år före nutid) ska vara i rimlig överensstämmelse med havsnivårekonstruktioner för samma tidsperiod; och iii) den euroasiatiska isen ska vid Saaleglaciationens maxskede vara påtagligt mäktigare än motsvarande is under den senaste glaciala cykeln (Weichselglaciationen).

Eftersom inlandsissimuleringarna är transienta innebär det att de variabler som används för att driva modellen, dvs klimat (lufttemperatur och nederbörd), havsnivå och avsmältning under shelfis, måste vara tidsberoende. Klimatdrivningen konstruerades genom att använda resultat från tre jämviktssimuleringar med en fullt kopplad global cirkulationsmodell av atmosfär och hav. Dessa jämviktssimuleringar representerar klimatet vid tre historiska tidpunkter: början av Saaleglaciationen (239 000 år före nutid), Saaleglaciationens maximum (140 000 år före nutid) och efter slutet av Saaleglaciationen (under interglacialen eem, ca 125 000 år före nutid). Klimatutvecklingen för tidsperioderna mellan dessa jämviktssimuleringar ansattes sedan med hjälp av geologiska data. Dessa data användes för att konstruera klimatindex vilka beskriver den tidsberoende utvecklingen av klimatet genom hela Saaleglaciationen.

Två referenskörningar, med 40 respektive 100 km rumslig upplösning, utfördes med inlandsismodellen. I körningen med 100 km upplösning uppnåddes den maximala istjockleken över Forsmark (ca 3 800 m) och Olkiluoto (ca 3 900 m) efter ca 110 000 år. Därefter följde en snabb avsmältning av den eurasiska isen under en tidsperiod på ca 10 000 år. I referenskörningen med 40 km upplösning blev istjockleken vid Forsmark och Olkiluoto ungefär 200 respektive 100 m mäktigare jämfört med motsvarande istjocklek i körningen med 100 km upplösning. Utöver referenskörningarna utfördes även känslighetssimuleringar med syfte att undersöka isens utbredning och tjocklek för olika i) klimatindex, ii) parametriseringar av lufttemperaturens avtagande med höjden, iii) parametrar relaterade till isens massbalans och iv) parametriseringar av kalvning och avsmältning under shelfis. Dessa simuleringar visade att endast simuleringarna med ändrad klimatindex hade stor inverkan på den transienta isutvecklingen. Totalt utfördes fyra känslighetssimuleringar med olika klimatindex, framtagna från olika geologiska arkiv. Endast två av dessa resulterade i istäckta förhållanden över Forsmark och Olkiluoto. De övriga två simuleringarna resulterade i isfria förhållanden över förvarsplatserna under hela Saaleperioden. Denna stora skillnad i isutveckling, beroende på klimatindex, belyser den stora osäkerhet som är kopplad till klimat- och inlandsisutvecklingen under Saaleglaciationen. I simuleringarna som utförts i denna studie bildas en inlandsis över östra Sibirien, vilken hänger ihop med den eurasiska och nordamerikanska inlandsisen. Existensen av en sådan östsibirisk inlandsis under Saaleglaciationen är mycket kontroversiell, även om den stöds av ett fåtal vetenskapliga studier. För att undvika att den kontroversiella östsibiriska inlandsisen på något sätt skulle påverka utvecklingen hos den eurasiska inlandsisen, infördes en artificiell värmekorridor mellan den östsiberiska isen och de angränsade isarna över Eurasien och Nordamerika, vilket hindrade att isarna sammanfogades.

Trots osäkerheterna beskrivna ovan uppvisar de genomförda simuleringarna en rimlig transient utveckling av Saaleglaciationen. Utveckling karakteriseras av en långsam isuppbyggnad följd av en relativt snabb deglaciation, en geografisk utbredning av den maximala iskonfigurationen som stämmer generellt väl överens med tolkningar av geologiska data, samt en betydligt mäktigare inlandsis över Eurasien än i rekonstruktioner av inlandsisen under Weichselperioden. Dessa simuleringar bedöms därför vara lämpliga att använda som randvillkor för att studera inverkan av en tidsberoende extrem-glaciation på spänningsförhållandet i berggrunden.

Contents

1 Introduction

A nuclear waste repository constructed at mid- to high latitudes, such as in northern Europe, Russia or Canada, will eventually be subject to glaciation (e.g. SKB 2010). The ice sheet will then increase the mechanical load on the repository, both through the additional weight of the ice itself and through the flexural response of the Earth's lithosphere. The flexure is important as it will induce horizontal stresses of the same magnitude as the vertical stress due to the weight of the ice. In addition to the increased stresses, the ice sheet will increase the water pressure in the rock below the ice. The increased pressure, in combination with the increased stresses, may cause the rock to fail, thereby causing disturbances ranging from local-scale increased fracture permeability to glacially induced earthquakes, such as the large faults in northern Sweden associated with the last deglaciation (e.g. Lagerbäck 1979). To improve the assessment of potential bedrock stress distributions resulting from future glaciations, it is important to account for the full range of possible Eurasian ice sheet configurations and evolutions suggested by geological records.

Previous ice-sheet modelling activities at SKB include a reconstruction of the Weichselian glaciation, which together with the Holocene interglacial constitutes the last glacial cycle (e.g. SKB 2010). The Weichselian reconstruction is in general agreement with contemporary Quaternary geological and geomorphological records (see e.g. SKB 2010), and has therefore been used as representative of a "typical" Late Pleistocene glaciation in SKB safety assessments. For instance, it has been used as reference glacial cycle in the safety assessment that supported the licence application for building the spent fuel repository at Forsmark in Sweden (SKB 2011).

The transient development of the Weichselian reconstruction has also been used as upper boundary condition in previous bedrock stress modelling activities (Lund et al. 2009). Despite its applicability, however, this reconstruction does not describe the most extreme ice sheets with respect to their spatial distributions and vertical extents. Therefore, relying only upon the Weichselian glacial cycle reconstruction does not account for the full range of potential ice sheets that could influence the bedrock stress distribution. Geological evidence suggest that the largest Quaternary Eurasian ice sheet existed during the penultimate, Saalian, glaciation, between ~ 241 000 and ~ 135 000 years before present (241–135 ka BP) during the Marine Isostope Stages 7e and 6 (hereafter denoted MIS 7e – MIS 6). During the peak of this glaciation, i.e. the Late Saalian glacial maximum, at ~ 140 ka BP (peak of MIS 6), it has been suggested that the Eurasian ice sheet extended approximately 200 km further south and 1 000 km further east compared to the Last Glacial Maximum (LGM) counterpart (Figure 1-1). Because of its massive size, the Saalian glaciation provides an excellent target period for evaluating the impact of large ice sheets on the bedrock stress distribution.

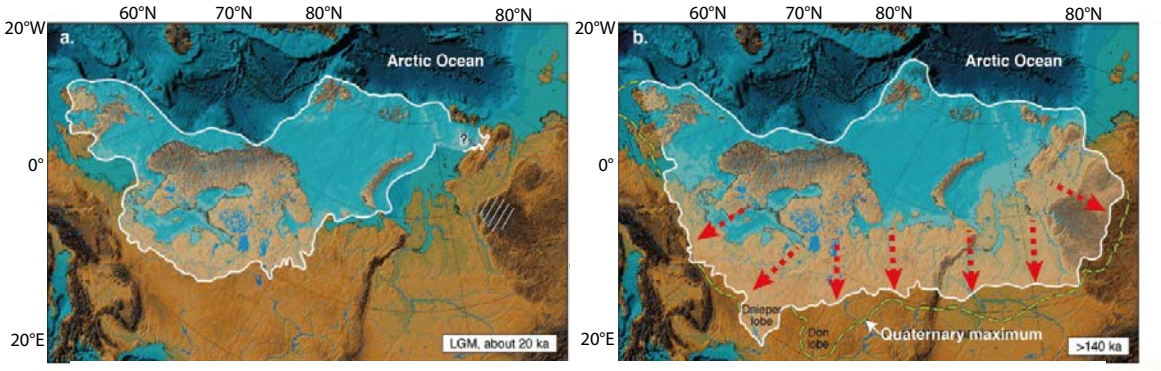

Figure 1-1. *Comparison of the Eurasian ice-sheet extent between (a) the Last Glacial Maximum (~ 21 ka BP) and (b) the Late Saalian (peak of MIS 6) glacial maximum (~ 140 ka BP; after Svendsen et al. 2004). Compared with the LGM Eurasian ice-sheet extent, the Late Saalian ice-sheet expands further south and east (b, red arrows). The largest LGM Eurasian ice-sheet reconstruction (ICE-5G, Peltier 2004) corresponds to an ice volume of ~ 22 m Sea level equivalent (SLE), which is about three times smaller than the Late Saalian Eurasian ice volume (~ 70 m SLE) as simulated by Peyaud (2006). Modified from Svendsen et al. (2004).*

The range of ice-sheet thicknesses over the Forsmark and Olkiluoto sites in Sweden and Finland have previously been thoroughly investigated in two dedicated studies (Colleoni et al. 2014a, Quiquet et al. 2016). Both studies conducted steady-state simulations of the peak Late Saalian Eurasian ice-sheet with the GRenoble Ice Shelf and Land Ice model (GRISLI; Ritz et al. 2001) using climate forcing derived from steady-state experiments, performed within the studies, with the NCAR CESM1.0.5 climate model (Gent et al. 2011). The study included an analysis of the effects of Eurasian climates simulated both with a large and small configuration of the North American ice sheet (Colleoni et al. 2014a). However, the range of Late Saalian ice-sheet thicknesses over Forsmark and Olkiluoto was investigated primarily by varying poorly constrained parameters in the ice sheet model. In the first study (Colleoni et al. 2014a), the ice thickness sensitivity to the parameter space was evaluated by means of uni-variate sensitivity experiments. In the second study (Quiquet et al. 2016), a Latin Hypercube Sampling (LHS) sampling technique was employed to conduct a multi-variate analysis of the parameter space in order to investigate its effect on the ice-sheet thickness. The combined result from the steady-state ice-sheet modelling experiments in Colleoni et al. (2014a) and Quiquet et al. (2016) suggests that the Late Saalian ice-sheet thickness over Forsmark and Olkiluoto was most likely around 3 500 m, whereas some simulations resulted in an ice thickness around 4 000 m.

Whilst the steady-state methodology employed in Colleoni et al. (2014a) and Quiquet et al. (2016) is sufficient, and sometimes even preferable, when investigating the sensitivity of model output variables to variations of intrinsic model parameters, the resulting equilibrium ice-sheet configurations with that strategy is not sufficient for bedrock stress modelling. Stress calculations depend on the deformation of lithosphere and asthenosphere beneath the ice sheet and in its peripheral area, which in turn depends on the spatio-temporal evolution of the ice sheets rather than theoretical steady-state configurations. Therefore, to enable more realistic calculations of the bedrock stress distribution based on the evolution of a large and thick ice sheet, transient ice-sheet simulations of the entire Saalian glacial cycle are conducted in the present study.

It is important to emphasise that the objective of this study is *not* to provide the most "realistic" ice-sheet evolution during the Saalian glacial cycle according to geological records. Instead the objective is to provide a *reasonable* ice sheet evolution that broadly conforms to the geological record. In particular, three conditions must be fulfilled for a transient ice-sheet evolution to qualify as "reasonable" in this context:

i) The ice sheet build-up and decay should exhibit an ice-sheet evolution typical for the last 800 ka, i.e. a relatively slow build-up to a maximum ice-sheet extent followed by a rapid deglaciation.

ii) The simulated Northern Hemisphere ice volume during the Late Saalian glacial maximum should be in reasonable agreement with contemporary sea-level reconstructions of that time (~ 80–140 m lower than at present).

iii) The ice sheet thickness over the repository sites Forsmark and Olkiluoto during the Late Saalian glacial maximum should be considerably greater than of the Weichselian maximum ice sheet thickness, reconstructed by SKB to be ~ 2 900 m over Forsmark (e.g. SKB 2010).

In the following chapter, the Saalian glacial cycle is briefly described. In Chapter 3, the climate forcing and experimental design of the transient of ice sheet model simulations are described. The results are presented in Chapter 4, followed by a discussion and the main conclusions in Chapters 5 and 6.

2 The Saalian glacial cycle (MIS 7e – MIS 6, ~ 241–135 ka BP)

The Saalian glacial cycle has rarely been investigated because of its unusual characteristics. MIS 7e (~ 248 – 233 ka BP) is considered an unusually cold interglacial compared with the other last four interglacials of the late Pleistocene (Dutton et al. 2009, Tzedakis et al. 2009, Masson-Delmotte et al. 2010), and the Late Saalian (peak of MIS 6) glacial maximum is considered one of the most, if not the most, extensive maxima that has occurred in Eurasia since the beginning of the Quaternary. However, no traces of this glaciation exist over North America as they were likely destroyed during the advance of the North American ice sheet towards the LGM (Dyke et al. 2002). On the Antarctic plateau, in the Pacific sector, the Saalian glacial cycle has been recorded as one of the coldest glaciations of the last 800 ka BP (Masson-Delmotte et al. 2010).

Climate proxies suggest that the Saalian glacial cycle differed substantially from the Weichselian glacial cycle in the following aspects:

1. From the global stack of benthic $\delta^{18}O$ record (Lisiecki and Raymo 2005), the Saalian glacial cycle starts with relatively high values (i.e. relatively cold conditions) but does not evolve towards as high isotopic values as during the Last Glacial Maximum (~ 21 ka BP, LGM) (Figure 2-1).
2. East Antarctica EPICA Dome C ice core records show that the beginning of the Saalian glacial cycle had lower atmospheric greenhouse gas concentrations (CO_2 and CH_4) than during the inception phase of last glacial cycle, whereas the Saalian glacial maximum had higher values of CO_2 and CH_4 than during the LGM (about 10 ppm difference) (Figure 2-1).
3. The orbital configuration, especially the relatively large precession index, resulted in predominately colder boreal summers and milder boreal winters during the Late Saalian glacial maximum compared with the LGM. As a consequence, the Late Saalian period holds a strong potential for extensive glaciations, especially over Eurasia (Colleoni et al. 2014b).
4. Past global-mean sea level reconstructions suggest that the global sea level during the Saalian glacial maximum could have been even lower than during the LGM (~ 120 m). However, the discrepancy between different sea-level reconstructions is large, both in terms of amplitude (between approximately 92 and 130 m; Rabineau et al. 2006, Rohling et al. 2017), and timing of the glacial maximum (between 134 and 139 ka BP; Dendy et al. 2017) (Figure 2-2). Both issues have been found to introduce substantial discrepancies in the interpretation of the Eemian sea level high stands (MIS 5e, 124–119 kys BP, Dutton et al. 2015) recorded in various locations around the world (Dendy et al. 2017, Rohling et al. 2017).

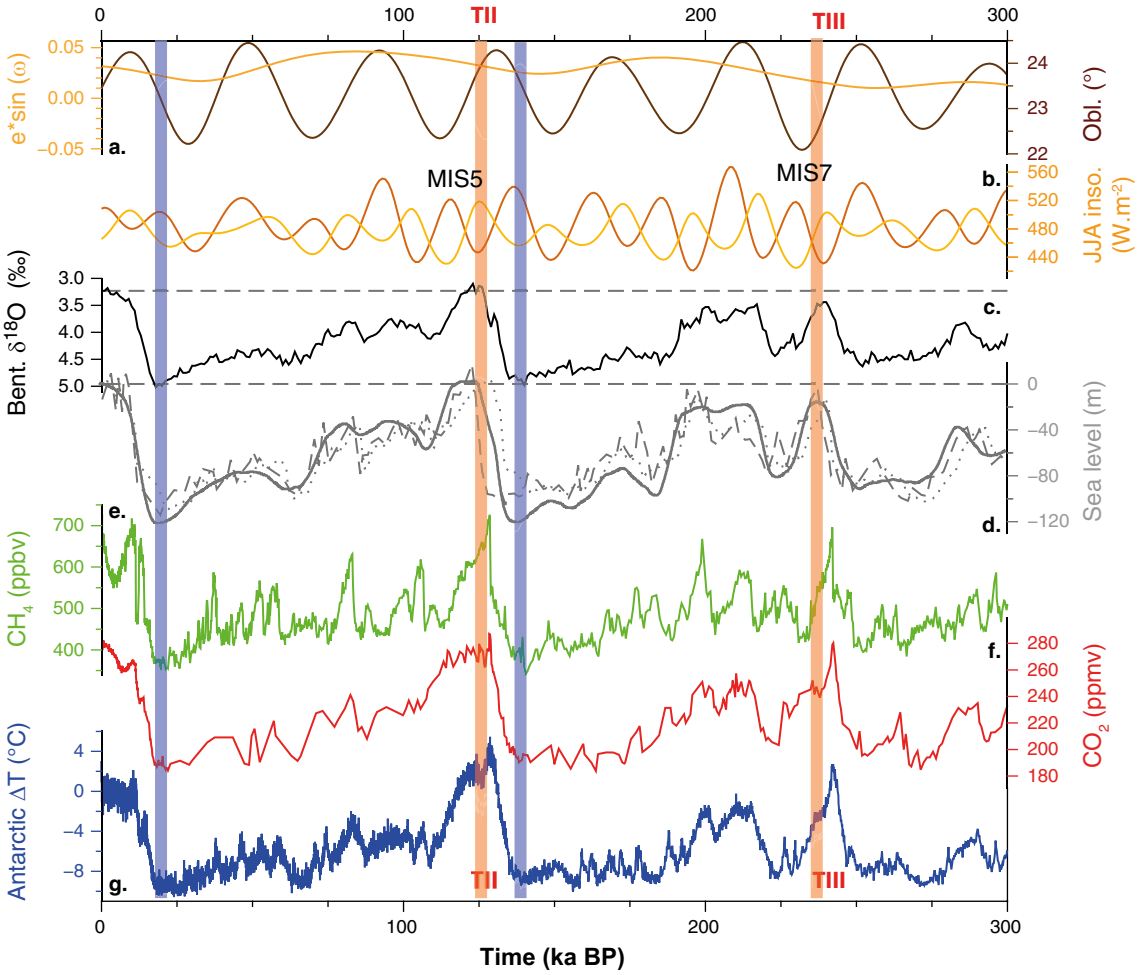

Figure 2-1. *Multi-proxy evolution over the last three glacial cycles: a. precession index and obliquity (°); b. Summer insolation at 65°N (light orange) and at 71°S (dark orange); c. benthic $\delta^{18}O$ global stack (Lisiecki and Raymo 2005); d. Past sea level reconstructions from Waelbroeck et al. (2002) (solid line), Siddall et al. (2003) (dashed line), Grant et al. (2014) (dotted line); e. EPICA Dome C methane ice core record (Loulergue et al. 2008); f. EPICA Dome C carbon dioxide ice core records (Lüthi et al. 2008); g. EPICA Dome C reconstructed air temperature record from Deuterium excess (Jouzel et al. 2007). Termination III and II, which refer to the end of MIS 8 and MIS 6 respectively, are indicated with orange vertical bars. The Late Saalian and last glacial maxima are indicated by vertical blue bars. The timings of the terminations and glacial maxima have been broadly defined based on the benthic $\delta^{18}O$ global stack in Lisiecki and Raymo (2005) (panel c). High (low) values of the benthic $\delta^{18}O$ global stack typically correspond to relatively cold (warm) conditions.*

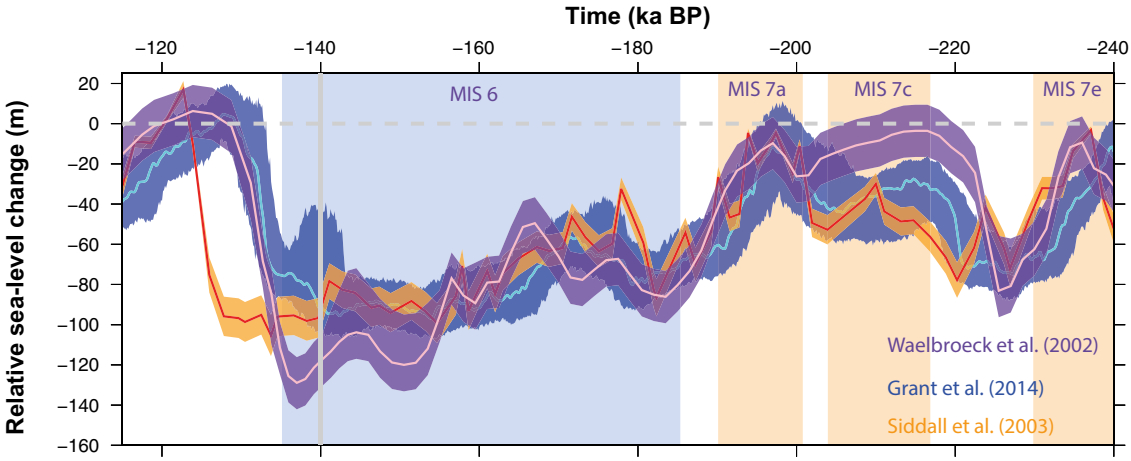

Figure 2-2. *Reconstructions of past relative sea-level changes inferred from $\delta^{18}O$ benthic records from North Atlantic (blue and orange; Waelbroeck et al. 2002, Siddall et al. 2003), and from planktonic foraminifera from the Red Sea (Grant et al. 2014). Shading corresponds to twice the standard error (2σ uncertainty). The dashed line shows the present-day sea-level (zero relative sea-level change) and the vertical line depicts the approximate timing of the Late Saalian glacial maximum at 140 ka BP.*

3 Methodology

As stated in the introduction, the objective of this study is to use transient ice sheet simulations for reconstructing the entire Saalian glacial cycle (MIS 7e – MIS 6) using the 3D thermomechanical ice sheet model GRISLI (Ritz et al. 2001). We use the same model version as in Colleoni et al. (2014a) and in Quiquet et al. (2016). A detailed description of the model and the setup of the steady-state simulations are provided in Colleoni et al. (2014a). In the following, we discuss the setup of the transient ice-sheet simulations.

3.1 Climate forcing

In contrast to steady-state simulations, transient ice-sheet model simulations require a representation of the temporal climate evolution. Here we carry out stand-alone ice-sheet model simulations meaning that no mutual interactions between the ice sheet and the climate evolution are considered. Representative time series of the temporal climate evolution are instead inferred from geological archives. Those time series are subsequently used to interpolate the climate conditions between simulated climate snapshots derived from steady-state Atmosphere Ocean General Circulation Model (AOGCM) simulations.

In this study, the climate evolution over the Saalian glacial cycle is interpolated between AOGCM simulated climate conditions corresponding to (i) a time close to the beginning of the cycle (at 239 ka BP), (ii) the glacial maximum (140 ka BP) and (iii) the peak of the cycle termination, i.e. towards 125 ka BP (Figure 3-1 and Table 3-1). In summary, the following climate snapshots were used:

1. **CS140 –** the glacial maximum 140 ka BP climate snapshot was simulated in Colleoni et al. (2014a) and later also used in Colleoni et al. (2016a)[1]. This snapshot uses the Late Saalian Eurasian ice sheet reconstruction from Peyaud (2006) (based on the reconstruction from Svendsen et al. 2004, see Figure 1-1) and a relatively small North American ice sheet compared to its LGM configuration. The choice of a smaller than LGM-sized North American ice sheet is motivated by the fact that the Late Saalian Eurasian ice sheet was larger than its LGM counterpart, whereas the total sea-level change during the Late Saalian glacial maximum was likely of similar magnitude to that of the LGM (see also Colleoni et al. 2014a). This snapshot was simulated using the CESM 1.0.5 atmosphere-ocean-sea-ice coupled configuration, on a finite volume grid of approximately $1 \times 1°$ horizontal resolution.
2. **CS239 –** a climate snapshot at 239 ka BP, corresponding to the beginning of the Saalian glacial cycle, used as initial condition for transient ice-sheet simulations. This snapshot was analysed and published in Colleoni et al. (2014b) and was carried out using the CESM 1.0.2 atmosphere-ocean-sea-ice coupled configuration, on a spectral grid of approximately $3° \times 3°$ horizontal resolution. This climate snapshot uses present-day topography and ice cover.
3. **CS125 –** a climate snapshot at 125 ka BP, corresponding to MIS 5e, used to end the transient simulations. This snapshot was analysed and published in Colleoni et al. (2014b) and was performed using the CESM 1.0.2 atmosphere-ocean-sea-ice coupled configuration, on a spectral grid of approximately $3° \times 3°$ horizontal resolution. This climate snapshot uses present-day topography and ice cover.

Ideally, one would like to utilise data from the same AOGCM for all time slices in order to avoid errors associated with inter-model biases and different model resolutions. However, as the availability of AOGCM simulations from the Saalian glacial cycle is extremely limited, this approach is not possible here. Despite this limitation, we anticipate that the uncertainty associated with errors in the AOGCMs is small compared to the uncertainty in temporal climate variability, see below.

[1] The CS140 climatic snapshot is referred to as "B140_Topo2" in Colleoni et al. (2014a) and Colleoni et al. (2016a). The name of this snapshot has been changed in the present report to be consistent with the naming of the other snapshots.

The surface air temperature and precipitation from all three snapshots are downscaled to present-day topography in the ice-sheet model grid using quadrant (inverse squared distance weighting) interpolation and a correction for the different surface elevations in the two models grids:

$$T_n(x,y) = T_n^{AOGCM}(x,y) + \lambda(S_n^{AOGCM}(x,y) - S_0(x,y)) \quad \text{Equation 3-1}$$

$$P_n(x,y) = P_n^{AOGCM}(x,y) \times \exp[\gamma(T_n^{AOGCM}(x,y) - T_n(x,y))] \quad \text{Equation 3-2}$$

where x and y, respectively, represent the Cartesian horizontal coordinates in GRISLI. For each climate snapshot (n = 125, 140, 239), the surface air temperature from the AOGCM (T_n^{AOGCM}) at a certain elevation (S_n^{AOGCM}) is downscaled to the present-day topography in GRISLI (S_0) according to a uniform atmospheric lapse rate (λ). The value of λ is in the downscaling procedure is set identical as in the ice-sheet model simulations (3.3 °C km^{-1} for annual mean and 4.1 °C km^{-1} for boreal summer mean, see Table 3-3). The resulting downscaled surface air temperature (T_n) is then used together with the temperature and precipitation from the AOGCM to compute the downscaled precipitation (P_n). The sensitivity of the downscaled precipitation to temperature changes is controlled by the precipitation factor (γ). The value of γ is set to 0.054 °C^{-1} for the downscaling procedure, i.e. the same as in the ice-sheet model simulations (Table 3-3). The downscaled temperature and precipitation fields in the Northern Hemisphere from all three AOGCM time slices are shown in Figure 3-2, Figure 3-3 and Figure 3-4.

An equivalent correction as in Equations 3-1 and 3-2 is also applied in GRISLI during runtime in response ice-sheet elevation changes:

$$T(x,y,t) = T_n(x,y) + \Delta T(x,y,t) + \lambda(S(x,y,t) - S_0(x,y)) \quad \text{Equation 3-3}$$

$$P(x,y,t) = P_n(x,y) \times \Delta P(x,y,t) \times \exp[\gamma(T(x,y,t) - T_n(x,y))] \quad \text{Equation 3-4}$$

where T and P refer to the annual-mean surface air temperature and precipitation, respectively, evolving during runtime in the ice-sheet simulations. ΔT and ΔP represent evolution of the surface air temperature and precipitation for the time periods between the time slices obtained from the AOGCM simulations. Between 239 ka BP and 140 ka BP, T_n and P_n in Equations 3-3 and 3-4 are given by the downscaled temperature and precipitation fields for 239 ka BP (i.e. index n = 239), and

$$\Delta T = (T_{140k} - T_{239k}) \times (1 - \alpha(t)) \quad \text{Equation 3-5}$$

$$\Delta P = \left(\frac{P_{140k}}{P_{239k}} - 1\right) \times \left(1 - \alpha(t)\right) + 1 \quad \text{Equation 3-6}$$

where $\alpha(t)$ is the climate index (see below). Equations 3-3 to 3-6 have the properties that $T = T_{140} + \lambda(S - S_0)$ if $\alpha = 0$ and $T = T_{239} + \lambda(S(t) - S_0)$ if $\alpha = 1$. Between 140 ka BP and 125 ka BP, n = 125 in Equations 3-3 and 3-4, and the temperature anomalies and precipitation factors are given by:

$$\Delta T = (T_{140k} - T_{125k}) \times (1 - \alpha(t)) \quad \text{Equation 3-7}$$

$$\Delta P = \left(\frac{P_{140k}}{P_{125k}} - 1\right) \times (1 - \alpha(t)) + 1 \quad \text{Equation 3-8}$$

such that $T = T_{140k} + \lambda(S - S_0)$ if $\alpha = 0$ and $T = T_{125} + \lambda(S - S_0)$ if $\alpha = 1$. To capture climate fluctuations on different time scales, it is common in stand-alone ice-sheet simulations to infer representative climate evolutions from available climate proxy data. For instance, for the Weichselian glacial cycle ice core records of δ^{18}O from the Greenland ice sheet are commonly used for that purpose. However, since no Greenland ice core records exist extending beyond the last interglacial (~ 128 ka BP), we used four other climate indices as representatives for the temporal climate evolution (Figure 3-1):

- Lisiecki and Raymo (2005) reconstructed the first long-term record of benthic δ^{18}O based on the stack of 57 worldwide sediment cores. However it was demonstrated that $\delta^{18}O_{benth}$ slightly lags the global ice volume evolution.

- Shakun et al. (2015) reconstructed a global stack of $\delta^{18}O_{sw}$ from sea water, which was shown to be more synchronous with ice volume changes than the benthic stack of $\delta^{18}O$. A caveat with this stack, as for other global stacks, is that it incorporates records from all over the globe and not only from Northern Hemisphere high latitudes. Therefore, this record is not entirely representative for the Northern Hemisphere climate evolution.
- Barker et al. (2011) produced a synthetic curve of Greenland $\delta^{18}O_{ice}$ evolution over the last 800 000 years based on a thermal bipolar seesaw model.
- Köhler et al. (2010) estimated the mean Northern Hemisphere air temperature based on the deuterium excess from EPICA dome C ice core records (East Antarctica).

The computation of the climate indices follows the approach in Charbit et al. (2002). Between 239 ka BP and 140 ka BP, the indices are calculated as:

$$\alpha(t) = \frac{CP(t) - CP(140k)}{CP(239k) - CP(140k)} \qquad \text{Equation 3-9}$$

and between 140 ka BP and 125 ka BP, they are given by:

$$\alpha(t) = \frac{CP(t) - CP(140k)}{CP(125k) - CP(140k)} \qquad \text{Equation 3-10}$$

CP corresponds to a given climate proxy record, and the resulting climate index *α(t)* from each record is shown in Figure 3-1. The climate indices are used in Equations 3-5 to 3-8 to compute the surface air temperature and total precipitation during runtime.

Table 3-1. Climate snapshots used to simulate ice-sheets evolution over the Saalian glacial cycle. The orbital parameters, i.e. eccentricity (Ecc), obliquity (Obl) and the date of perihelion are reported for each climate snapshot. Modern orbit has Ecc = 1.7 %, Obl= 23.44 and a perihelion on January 4. Pre-industrial greenhouse gases are CO_2 = 284 ppm, CH_4 = 791 ppbv and N_2O = 276 ppbv. References: [1] Colleoni et al. (2014b), [2] Colleoni et al. (2014a), [3] Colleoni et al. (2016a).

ID	Ecc (%)	Obl (°)	Perihelion	CO_2 (ppmv)	CH_4 (ppbv)	N_2O (ppbv)	Resolution	Model release	Ref.
CS239	3.6	22.70	12 July	245	565	267	Spectral T31 ~ 3°	CESM 1.0.2	[1]
CS140	3.3	23.42	6 December	192	401	217	Finite volume 0.9° x 1.25°	CESM 1.0.5	[2][3]
CS125	4.0	23.80	23 July	276	640	263	Spectral T31 ~ 3°	CESM 1.0.2	[1]

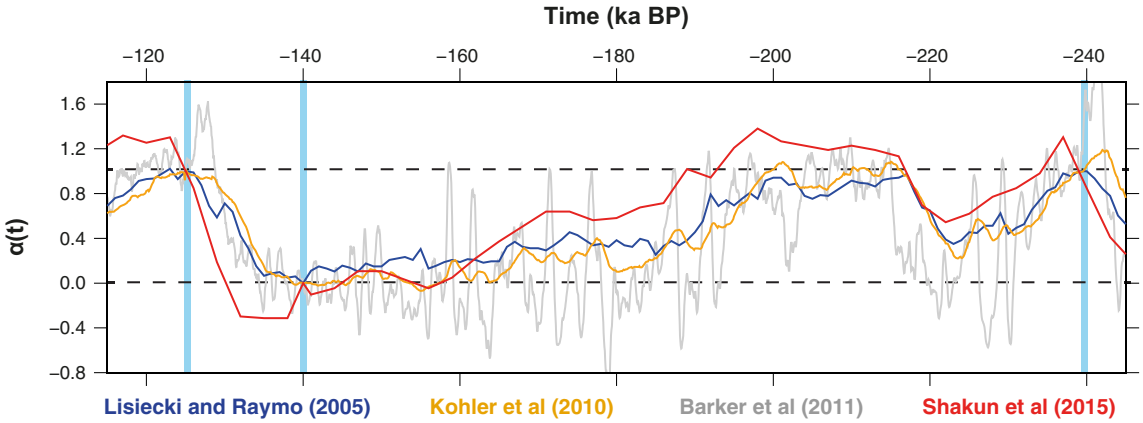

Figure 3-1. *Climate indices, based on different geological records (indicated by colours), used to interpolate the transient evolution of surface air temperature and precipitation between the three climate snapshots (indicated by vertical light blue bars) referred to as "CS239", "CS140" and "CS125". For more information on the climate snapshots and the calculation of the climate indices, see the text.*

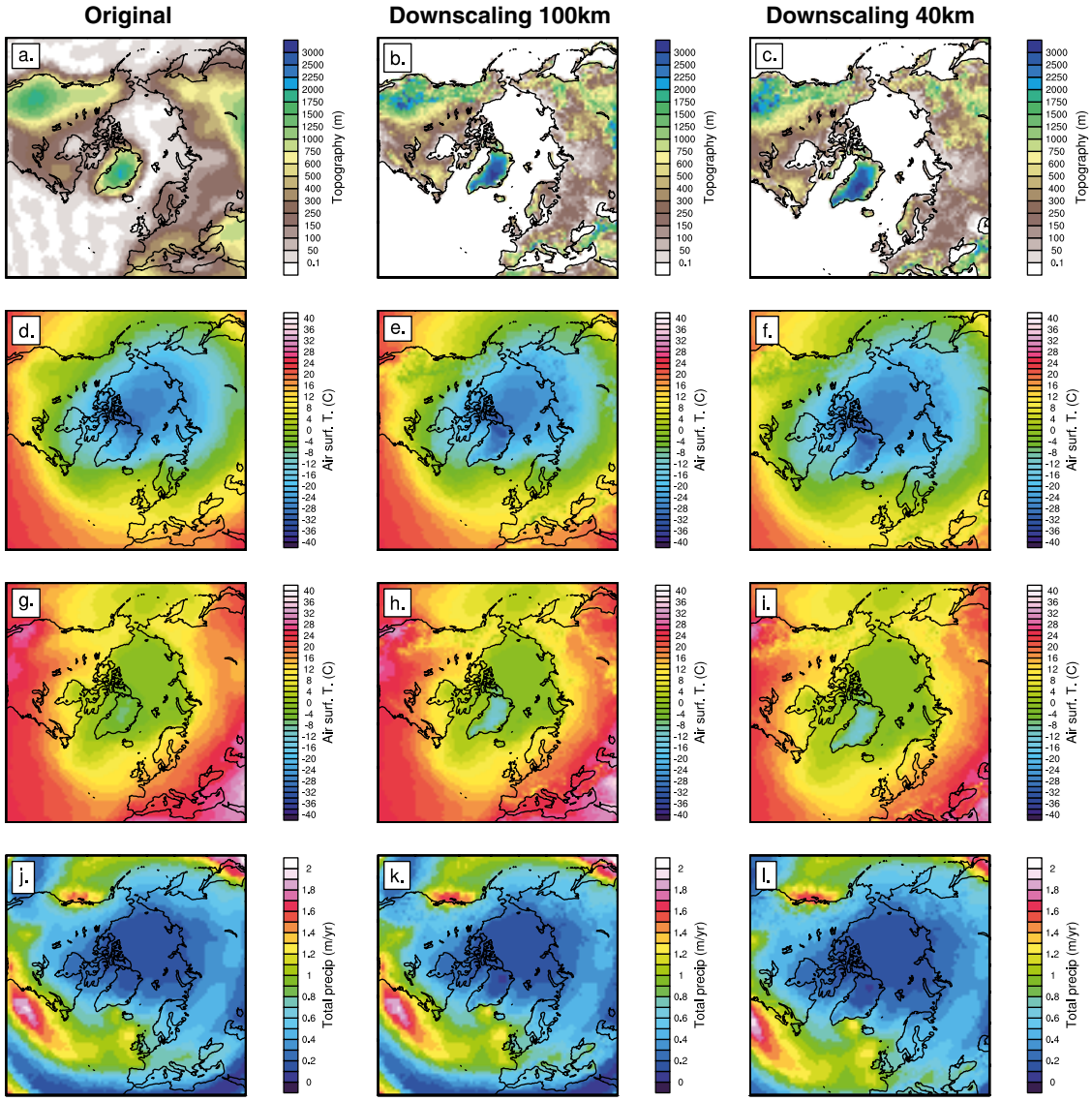

Figure 3-2. *Downscaling of the CS239 climate snapshot on the different ice sheet model grids used in the present study, using a lapse rate of 3.3 °C km^{-1} for annual mean and 4.1 °C km^{-1} for boreal summer mean and a precipitation factor of 0.054 °C^{-1}, see Equations 3-1 and 3-2, and the text.. From top to bottom: Topography (m); Annual mean air surface temperature (°C); July surface air temperature (°C) and Annual precipitation (m a^{-1}). Present-day topography is derived from ETOPO1 (Amante and Eakins 2009).*

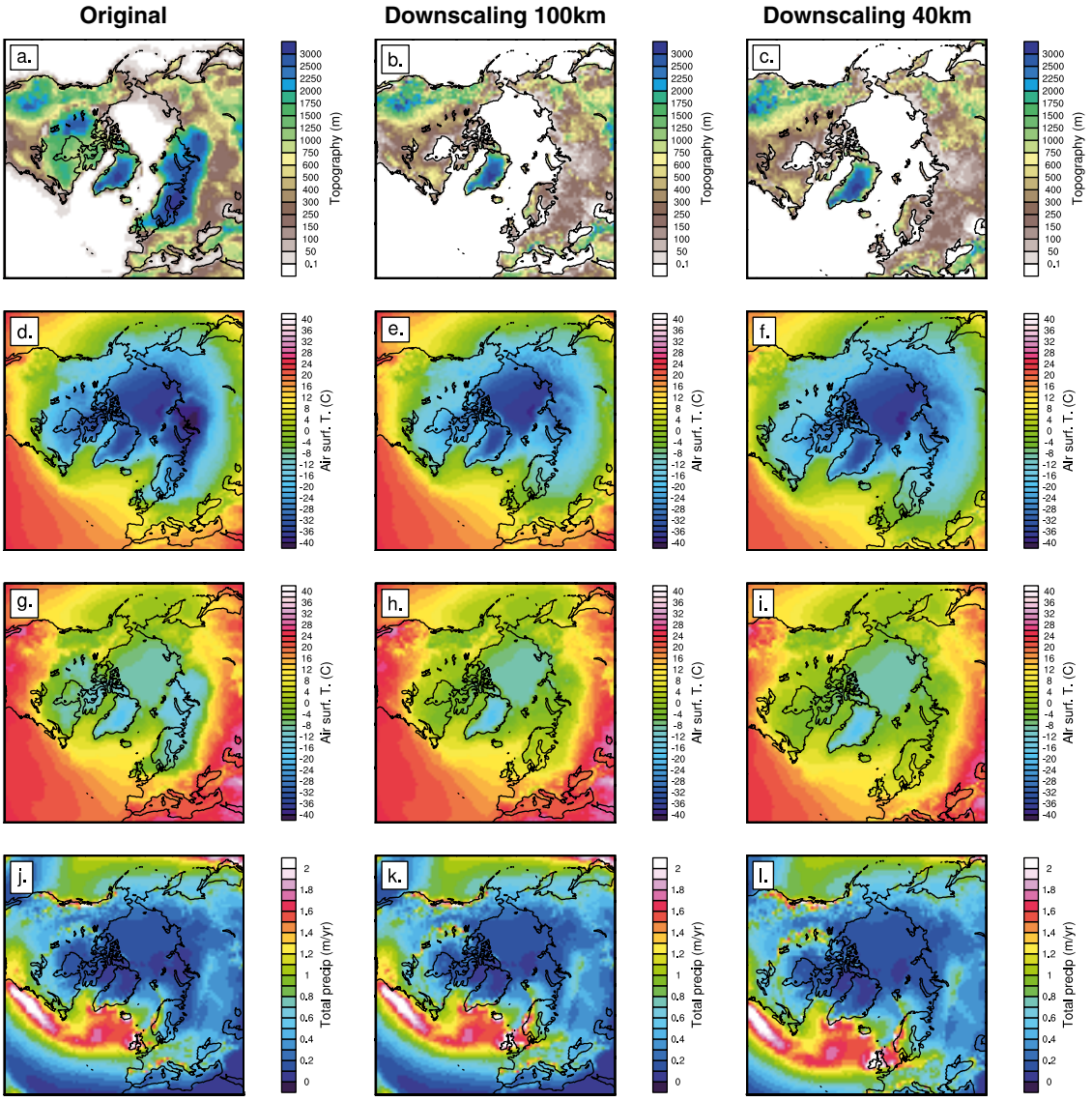

Figure 3-3. *Downscaling of the CS140 climate snapshot on the different ice sheet model grids used in the present study, using a lapse rate of 3.3 °C km^{-1} for annual mean and 4.1 °C km^{-1} for boreal summer mean and a precipitation factor of 0.054 °C^{-1}, see Equations 3-1 and 3-2, and the text.. From top to bottom: Topography (m); Annual mean air surface temperature (°C); July surface air temperature (°C) and Annual precipitation (m a^{-1}). Present-day topography is derived from ETOPO1 (Amante and Eakins 2009).*

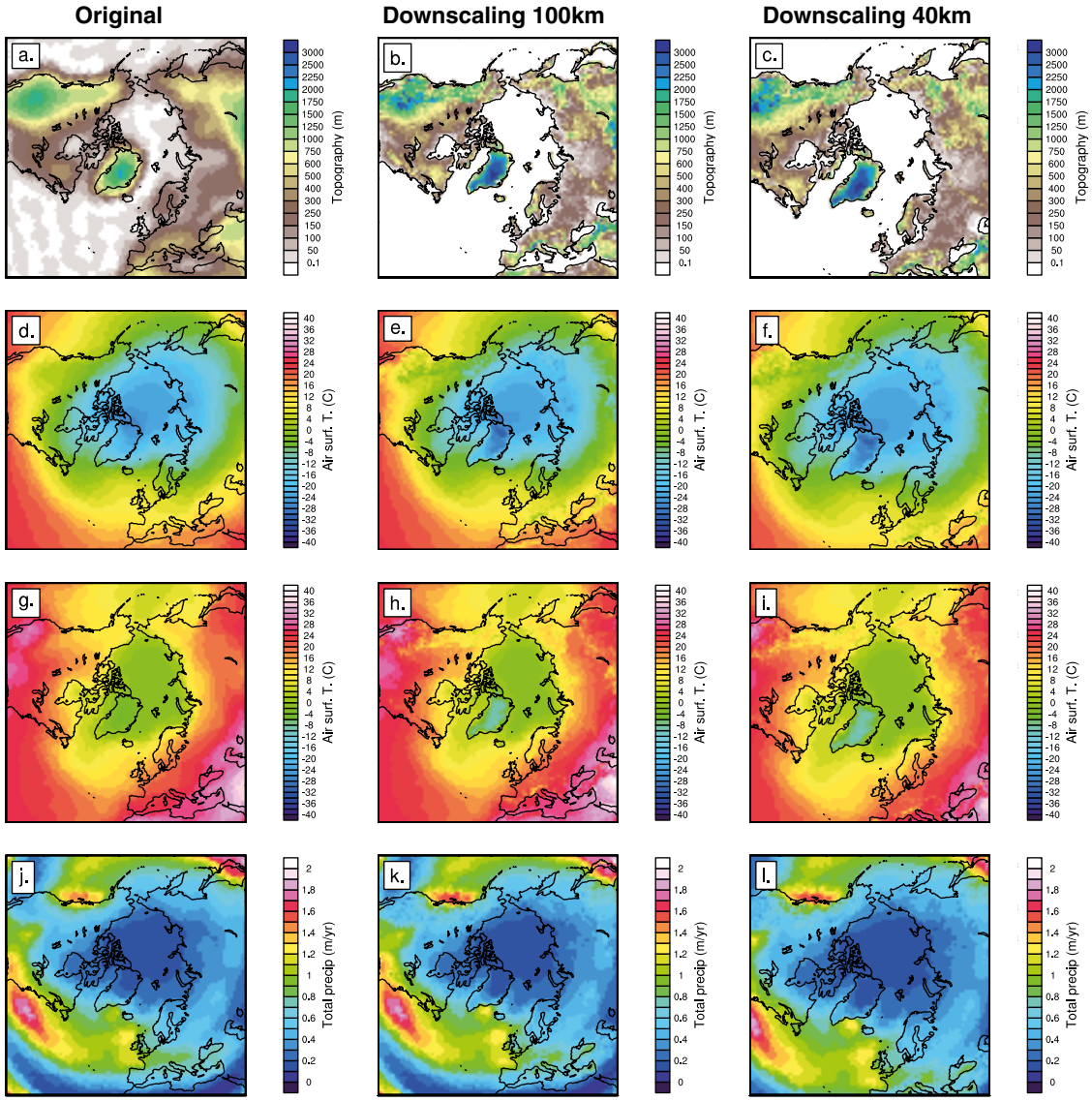

Figure 3-4. *Downscaling of the CS125 climate snapshot on the different ice sheet model grids used in the present study, using a lapse rate of 3.3 °C km^{-1} for annual mean and 4.1 °C km^{-1} for boreal summer mean and a precipitation factor of 0.054 °C^{-1}, see Equations 3-1 and 3-2, and the text.. From top to bottom: Topography (m); Annual mean air surface temperature (°C); July surface air temperature (°C) and Annual precipitation (m a^{-1}). Present-day topography is derived from ETOPO1 (Amante and Eakins 2009).*

3.2 Experiments

The ice-sheet model experiments conducted in this study are summarized in Table 3-2. The numerical values of the ice-sheet model parameters used in the control simulation (*NH_CTL*), are shown in Table 3-3. The set of parameters in Table 3-3 were used in one ensemble in the Latin Hypercube experiments in Quiquet et al. (2016). This simulation resulted in a steady-state ice-sheet thickness of ~ 3 500 m over the Forsmark and Olkiluoto sites, similar to the average ice thickness in the Latin Hypercube ensemble. The influence of using parameter combinations from the Latin Hypercube ensemble that resulted in the thickest ice sheets, with thicknesses greater than ~ 4 000 m at the Forsmark and Olkiluoto sites, on the transient Saalian ice-sheet evolution is discussed in Section 5.2. For more information on how the parameters in Table 3-3 are treated in GRISLI, see Colleoni et al. (2014a) and Quiquet et al. (2016).

The control simulation *NH_CTL* is performed using the Shakun et al. (2015) climate index (Figure 3-1). However, to evaluate the sensitivity of the Saalian ice-sheet evolution to the transient climate development, we also conduct three sensitivity simulations with the other climate indices featured in Figure 3-1. These simulations, referred to as NH_BAR, NH_LIS and NH_KOH (Table 3-2), use the same parameters as in *NH_CTL* (Table 3-3). Three sensitivity cases were also constructed for testing the impact of surface mass balance (SMB)-related parameters and transient calving and sub-shelf melting. Specifically, these experiments analyse the sensitivity of the ice-sheet evolution to a different parameterization of the atmospheric lapse rate (*NH_λ*), another refreezing scheme for the Positive Degree Day (PDD) ablation model (*NH_PDD*), and a different methodology for computing sub-ice shelf melting and transient calving (*NH_OCE*).

In addition, one sensitivity case was also constructed to test the impact of the connection between the Siberian ice sheet and the Eurasian ice sheet. In the simulations presented here, an ice sheet grows over Eastern Siberia, reaching a maximum ice volume of nearly 30 m sea-level equivalents (SLE) in some simulations. It has been shown that the surface air temperature in this area is sensitive to the atmospheric stationary wave field, which is largely controlled by the ice-sheet topography during glaciations (Colleoni et al. 2016a, Liakka et al. 2016, Liakka and Löfverström 2018). Therefore, small changes in the stationary waves field, due to e.g. changes in the size of the North American ice sheet, may enable ice to nucleate in the region (e.g. Liakka et al. 2016). However, whether or not an ice sheet existed in Eastern Siberia during the Saalian glacial cycle remains debated. Analyses of geological evidence in the East Siberian Sea (Niessen et al. 2013) have suggested that grounded ice flowed in this area and that an ice shelf could have formed. In addition, a recent interpretation of sediment cores from the same area suggests that thick sea ice was covering the East Siberian Sea (Stein et al. 2017). From a dynamical point of view, it is difficult to imagine the development of an ice shelf without any feeding from a grounded ice sheet. This is however still a matter of debate since sheet models easily can tune their parameters to cover this area with ice sheets and ice shelves. Since the geological evidence are uncertain and do not provide information on potential dimension and volume of the Siberian ice sheet, if it existed, we choose to impose a heat corridor to separate the Eurasian ice sheet from the Siberian ice sheet and to exclude the accumulated East Siberian ice from our calculations of Northern Hemisphere ice volume.

The simulations are initiated at 245 ka BP, i.e. slightly earlier than 239 ka BP, to provide a short spin-up time before the start of the Saalian glacial cycle. The reason for the short initial spin-up is that small areas were likely still glaciated at the end of MIS 8 (Colleoni et al. 2014b). However, since we do not have any climate snapshots corresponding to this time period, we use CS239 modulated by the climate index prior to 239 ka BP. The simulations are chosen to end approximately 20 ka after the termination of the Saalian glacial cycle in order to account for the fact that the peak of glacial maximum occurs at different times in the different indices used in this study (Figure 3-1).

As a first step, to test the accuracy and efficiency of the transient method, simulations were carried out over a Northern Hemisphere model domain using a low horizontal resolution of 100 km. The low resolution allows us to test various hypotheses and adjust model parameters. This is further detailed and discussed in Sections 4.1 and 4.2. As a second step, the horizontal resolution is refined to 40 km over the Northern Hemisphere for the control simulation (Table 3-2) with the aim to produce results that subsequently will be used for bedrock stress modelling within another study. The evolution of the ice-sheet thickness over Forsmark and Olkiluoto from these simulations is briefly presented in Section 4.2.

Table 3-2. List of ice sheet model simulations carried out in the present study. The model domain covers the Northern Hemisphere. All simulations use the parameter values presented in Table 3-3 unless otherwise stated.

RUN ID	Hor. Res. (km)	Climate index (Figure 3-1)	Sibieran ice sheet connection	Transient Ocean melt	Transient calving	PDD refreeze	Elev. dep. lapse rate
NH_CTL	100	Shakun et al. (2015)					
NH_BAR	"	Barker et al. (2011)					
NH_KOH	"	Köhler et al. (2010)					
NH_LIS	"	Lisiecki and Raymo (2005)					
NH_λ	"	Shakun et al. (2015)					X
NH_OCE	"	Shakun et al. (2015)		X	X		
NH_PDD	"	Shakun et al. (2015)				X	
NH_SIB	"	Shakun et al. (2015)	X				
NH40_CTL	40	Shakun et al. (2015)					

Table 3-3. Ice-sheet model parameters values used in this study: λ is the atmospheric lapse rate (°C km^{-1}), γ the precipitation factor (‰), σ the amplitude of daily temperature cycle (°C), γ_{GHF} the geothermal heat flux (GHF) modificator, C_{snow} the melting coefficient for snow (mm day^{-1} °C^{-1}), C_{ice} the melting coefficient for ice (mm day^{-1} °C^{-1}), P_{solid} the temperature threshold for snow (°C), d the thickness thickness of the thermo-active layer in the surface mass balance model, Cf the dragging coefficient, and EF the enhancement factor for SIA. The GHF modificator, γ_{GHF}, is multiplied with a baseline GHF distribution by Shapiro and Ritzwoller (2004) to obtain the actual GHF used in the model. For a broader discussion on how these parameters are treated in the ice-sheet model, see Colleoni et al. (2014a) and Quiquet et al. (2016). For a description of how the parameter values were selected, see the text.

Parameter	Value
λ (°C km^{-1})	Annual: 4.1, Summer: 3.3
γ (°C^{-1})	0.054
σ (°C)	2.24
γ_{GHF}	1.072
C_{snow} (mm day^{-1} °C^{-1})	2.3
C_{ice} (mm day^{-1} °C^{-1})	7.7
P_{solid} (°C)	−0.75
d (m)	1.85
C_f	4.35×10^{-5}
EF	3.38

4 Results

4.1 Northern Hemisphere ice-sheet evolution

In the following sections, the main results from the simulations with 100 km resolution in Table 3-2 are presented and discussed. First, we present results from the control simulation in Section 4.1.1. Thereafter we evaluate the sensitivity of the Northern Hemisphere ice volume and ice extent to the choice of climate index (Section 4.1.2), various surface mass balance (SMB) parameters and parameterizations (Section 4.1.3), different parameterization of sub-ice shelf melting and transient calving (Section 4.1.4) and a physical connection between the East Siberian and adjacent ice sheets (Section 4.1.5). The resulting maximum Northern Hemisphere ice volume and maximum ice thickness at the Forsmark and Olkiluoto sites from these simulations are summarized in Table 4-1.

Table 4-1. Simulated maximum Northern Hemisphere ice volume (m Sea Level Equivalents; SLE), Eurasian and Siberian ice volume (m SLE) as well as maximum ice thickness (m) and bedrock depression at the Forsmark and Olkiluoto sites for each of the simulations in Table 3-2. Note that the Siberian ice sheet has been excluded from the calculations of the maximum Northern Hemisphere ice volume, see the text.

RUN ID	Max. Northern Hemishere ice volume (m SLE)	Max. Eurasian ice volume (m SLE)	Max. Siberian ice volume (m SLE)	Max. ice thickness (m) – Forsmark	Max. bedrock depression (m) – Forsmark	Max. ice thickness (m) – Olkiluoto	Max. bedrock depression (m) – Olkiluoto
NH_CTL	−128	−55	−28	3820	−920	3910	−960
NH_BAR	−110	−50	−26	3450	−690	3230	−680
NH_KOH	−86	−35	−20	900	−120	40	−60
NH_LIS	−71	−24	−17	~ 0	−70	0	0
NH_λ	−111	−49	−26	3750	−890	3820	−930
NH_OCE	−131	−57	−27	3870	−930	3970	−980
NH_PDD	−113	−50	−26	3790	−900	3850	−930
NH_SIB	−118	−50	−29	3770	−900	3840	−940
NH40_CTL	−130	−53	−25	4030	−950	4040	−970

4.1.1 Control simulation

The simulation using the parameters in Table 3-3 and the climate index based on Shakun et al. (2015) global stack of $\delta^{18}O_{sw}$ is here considered as the reference transient ice-sheet model simulation, i.e. the control simulation (*NH_CTL*, Table 3-2). This simulation also includes the separation of the Eurasian ice sheet from the Siberian ice sheet (see previous section).

The simulated Northern Hemisphere ice volume in *NH_CTL* remains relatively low until ~ 165 ka BP, underestimating the ice volume with respect to proxy data by up to ~ 70 m SLE around 180 and 230 ka BP (Figure 4-1). Subsequent to ~ 165 ka BP, the simulated Northern Hemisphere ice volume begins to increase significantly until its maximum value is reached at around 135 ka BP (Figure 4-1a). The peak NH ice volume amounts to 128 m SLE (Figure 4-1a, Table 4-1), with 55 m SLE for the Eurasian ice sheet and 70 m SLE for the North American ice sheet (Figure 4-1b, Table 4-1). The maximum change in ice volume (with the Siberian ice sheet excluded) is hence within the 80–140 m SLE range suggested by the geological evidence (Figure 2-2).

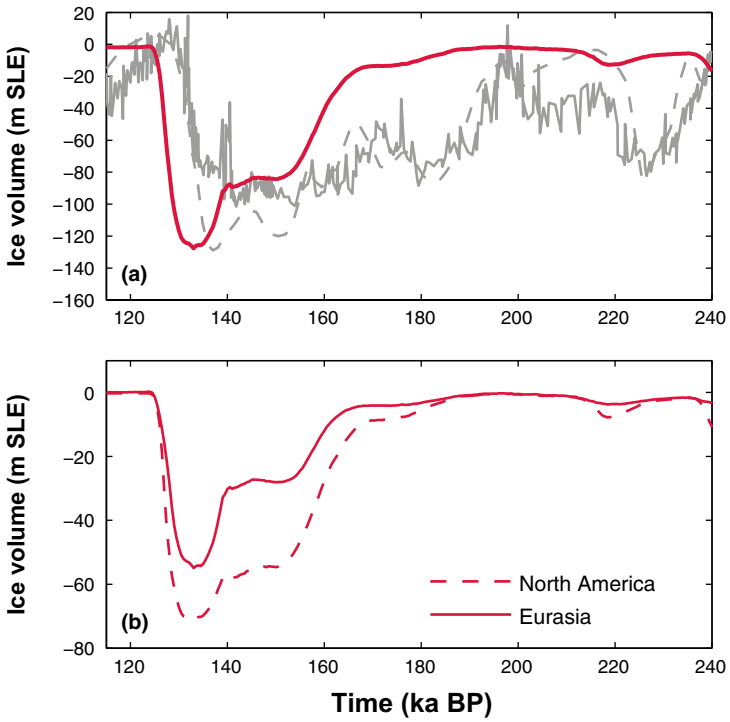

Figure 4-1. *Simulated transient ice volume evolution (m SLE) in the control simulation NH_CTL (Table 3-2). a. Northern Hemisphere ice volume, excluding the Siberian ice sheet (see Section 3.2 and Section 4.1.5). b. individual ice volume for Eurasian and North American ice sheets. Grey solid and dashed curves correspond to Grant et al. (2014) and Waelbroeck et al. (2002) sea level reconstructions, respectively.*

The spatial distribution of the ice thickness at six key time slices of *NH_CTL* is shown in Figure 4-2. Glacial inception occurs over the common nucleation sites for Arctic glaciations, i.e. over the Canadian archipelago for the North American ice sheet and over the islands of the Barent and Kara Seas for the Eurasian ice sheet (Figure 4-2a). The North American ice sheet expands slowly southward and two main domes forms West and East of the Hudson Bay (Figure 4-2c), consistent with the early expansion reconstructed for the Weichselian glacial cycle (e.g. Kleman et al. 2013). The Eurasian ice sheet first develops over Russia (Figure 4-2b) and accumulates over Scandinavia towards ~ 160 ka BP (Figure 4-2c). Thereafter, the Eurasian ice sheet spreads over the Russian plains and Western Europe until 133 ka BP, at which point the maximum extend is reached (Figure 4-2d). The retreat of both ice sheets is fast: they have terminated completely by ~ 123 ka BP (Figure 4-2f), consistent with the timing of the imposed climate index (Shakun et al. 2015, see Figure 3-1). Sea level proxies indicate the maximum MIS 5e sea level high-stand occurred at some point between 128 and 125 ka BP (Dendy et al. 2017).

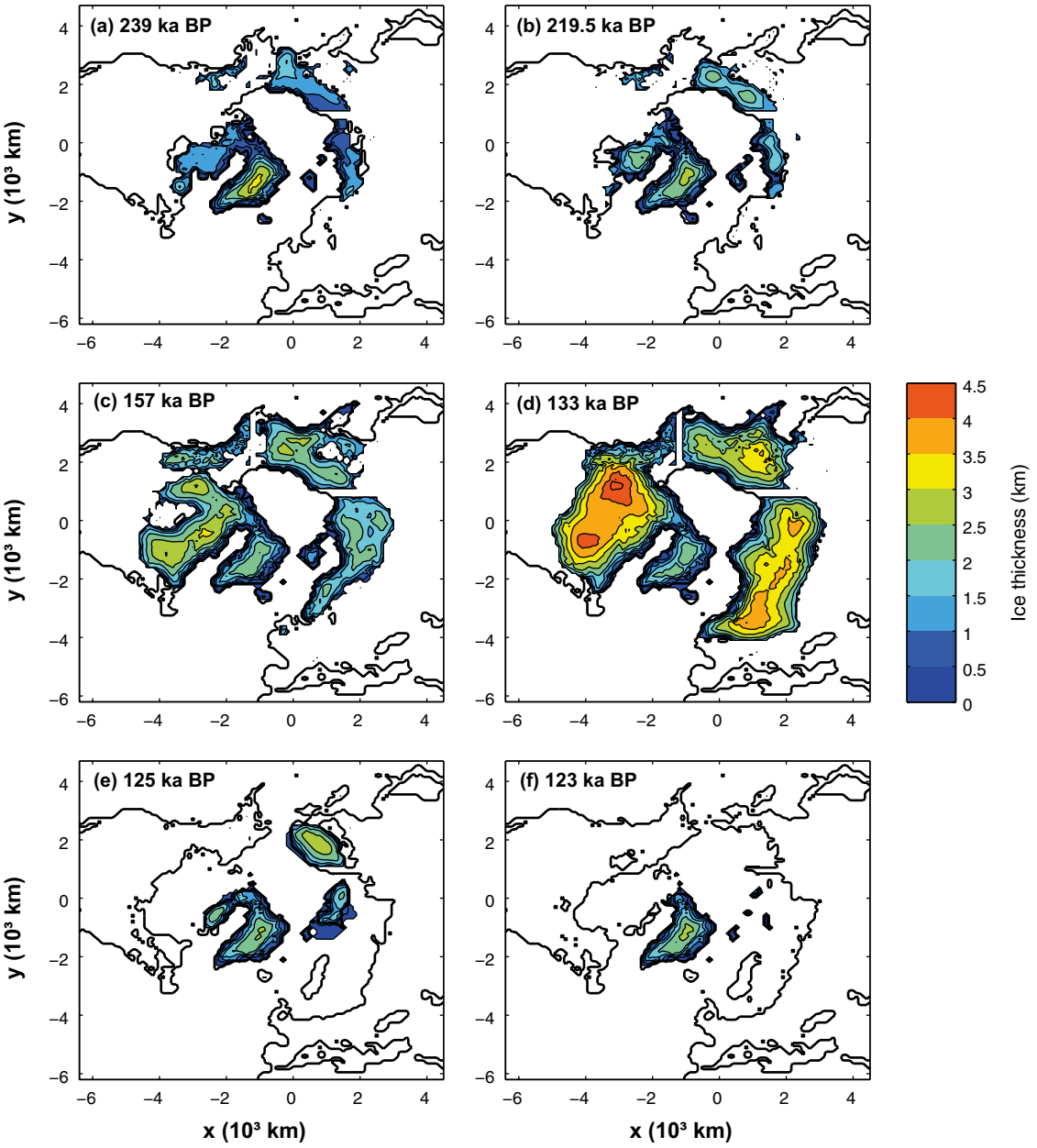

Figure 4-2. *Transient evolution of ice thickness (m) in the control simulation NH_CTL (Table 3-2). Glacial maximum is reached at 133 ka BP.*

4.1.2 Impact of climate index

As previously mentioned, the climate index determines the pathway of the ice sheet evolution in transient stand-alone simulations. The simulated ice volume evolution resulting from different indices (Figure 3-1) is displayed in Figure 4-3. In addition to *NH_CTL*, which uses the Shakun et al. (2015) climate index, Figure 4-3 hence shows the *NH_BAR*, *NH_KOH* and *NH_LIS* simulations (Table 3-2).

The index calculated from Barker et al. (2011) is based on Greenland ice core records. This index has a relatively high temporal resolution for the timescales considered here (Figure 3-1). This is not the case with the other indices that are derived from geological archives with lower temporal resolutions. As a result, there is a significant millennial variability of the transient ice volume evolution *NH_BAR* which is not present in the simulations using the other indices (Figure 4-3). The maximum ice volume change in *NH_BAR* amounts to 110 m SLE, i.e. slightly lower than the maximum ice-volume change in *NH_CTL* (128 m SLE) but about 20 and 40 m SLE higher than in *NH_KOH* and *NH_LIS*, respectively (Table 4-1).

Similar to the maximum ice volume, the timing of the maximum Eurasian ice-sheet extent also varies significantly among the simulations with different climate indices (Figure 4-3). While *NH_CTL* results in a maximum Eurasian ice-sheet extent at 133 ka BP, *NH_BAR* has its maximum at 150 ka BP, *NH_LIS* around 139 ka BP and *NH_KOH* at 142 ka BP.

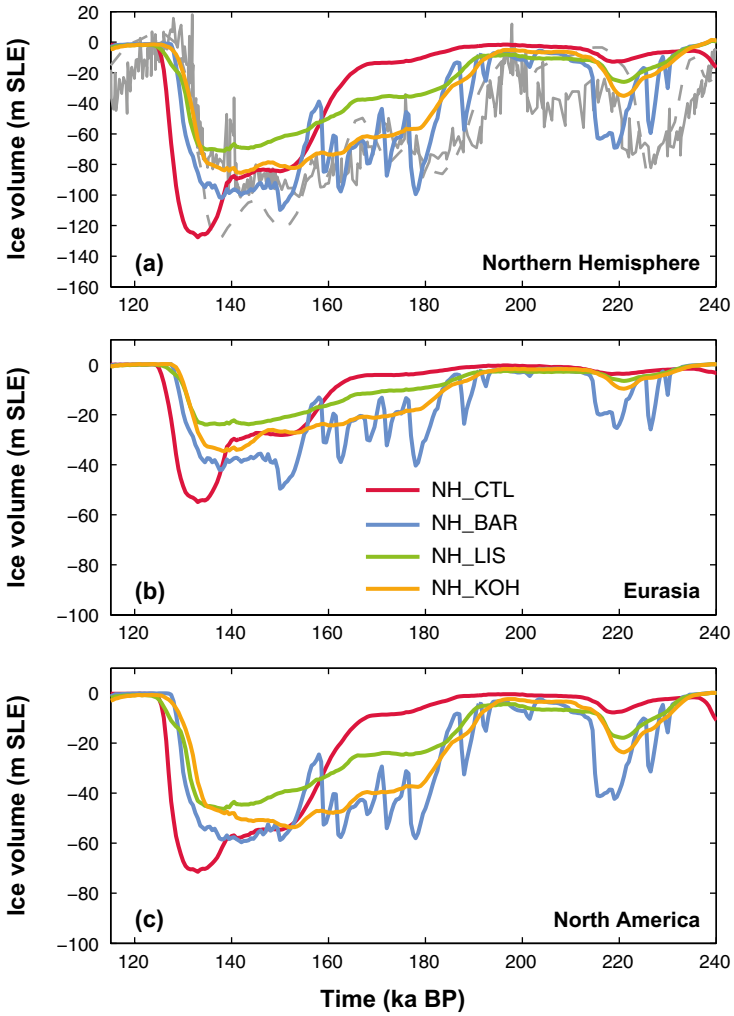

Figure 4-3. *Comparison of the effect of the four different climate indices (Figure 3-1) used in the present study on the simulated transient evolution of ice volume. Red: Shakun et al. (2015); Orange: Barker et al. (2011); Blue: Lisiecki and Raymo (2005); Purple: Köhler et al. (2010). Top: Northern Hemisphere ice volume excluding the Siberian ice sheet; Middle: Eurasian ice sheet ice volume; Bottom: North American ice volume. Ice volumes are given in m SLE and are compared the sea level reconstructions from Grant et al. (2014) (grey solid line) and Waelbroeck et al. (2002) (grey dashed line).*

Consistent with the large spread in simulated ice volumes obtained with the different indices, not all the simulations yield an extensive Eurasian ice sheet (Figure 4-4). Only the *NH_CTL* and *NH_BAR* simulations result in fully glaciated conditions over the repository sites at some point during the glacial cycle. Therefore only results from those simulations are considered as potential input to the bedrock stress modelling. The transient evolution of the Northern Hemisphere ice sheets at six key time slices in *NH_CTL* and *NH_BAR* is shown in Figure 4-2 and Figure 4-5, respectively.

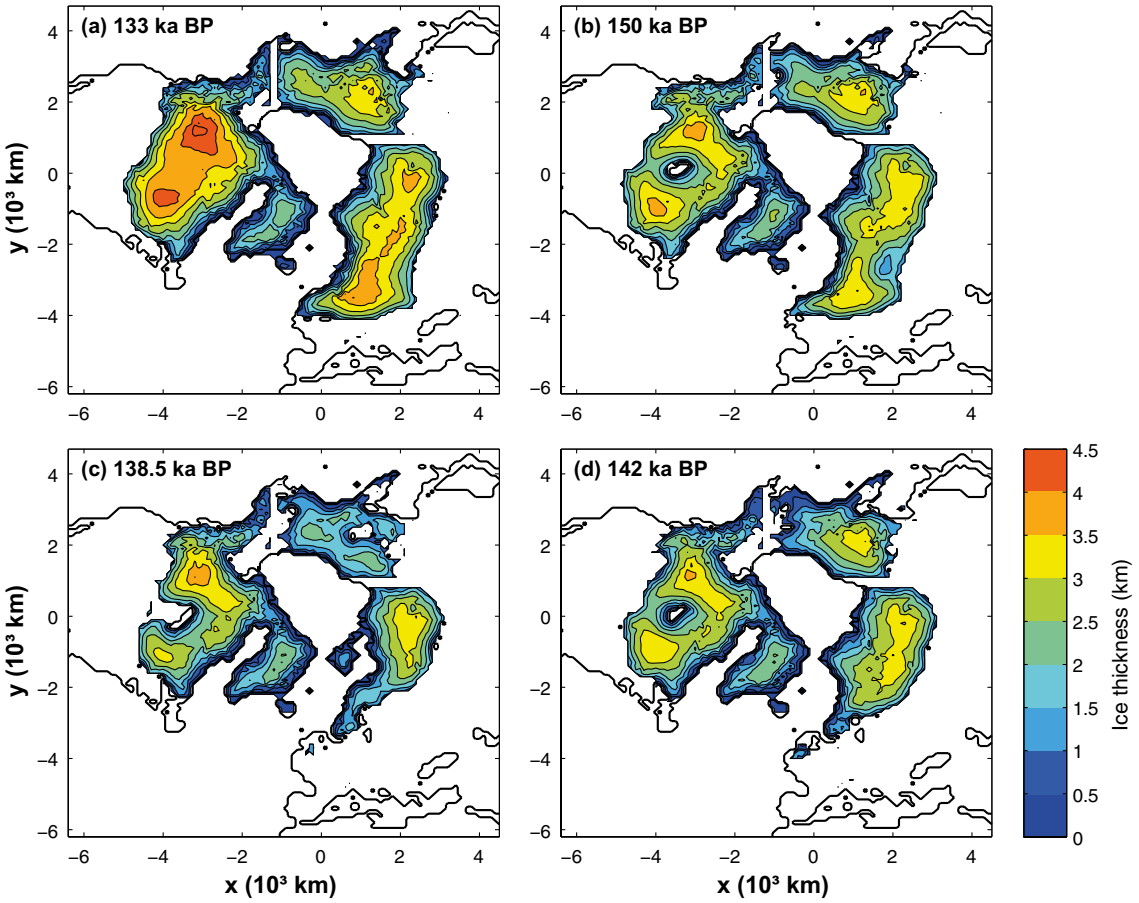

Figure 4-4. *Ice thickness at time of Eurasian glacial maximum in the simulations with different climate indices (Figure 3-1): (a) NH_CTL, (b) NH_BAR, (c) NH_LIS and (d) NH_KOH. Note that the timing of glacial maximum is different for each of the four simulations.*

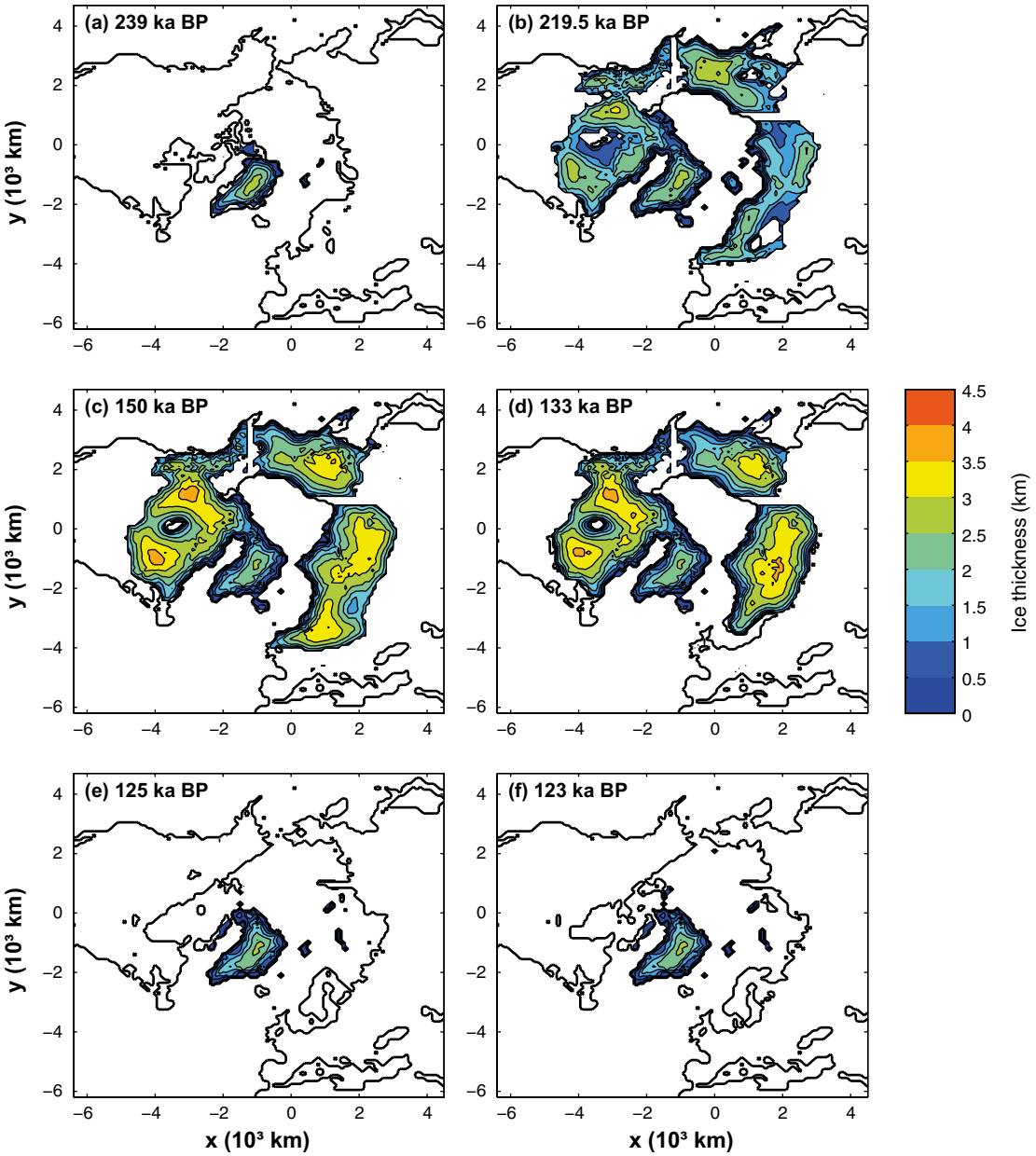

Figure 4-5. *Transient evolution of ice thickness (m) in NH_BAR (Table 3-2). Glacial maximum is reached at 150 ka BP.*

4.1.3 Impact of SMB-related parameters

As illustrated in the previous section, the temporal changes in climate, here controlled by the climate indices, strongly modulates the surface mass balance (SMB) and hence also the transient ice-sheet evolution (Figure 4-3). In this section, we also evaluate the sensitivity of the Eurasian ice sheet to parameters related the SMB. Since the previous SKB studies on the Late Saalian ice-sheet thickness (Colleoni et al. 2014a, Quiquet et al. 2016) have already conducted uni-variate and multi-variate analyses of many SMB-related parameters (e.g. lapse rate values, precipitation factor and temperature threshold for snow), we test different aspects of the SMB in the present study.

First, we evaluate the impact of an elevation-dependent lapse rate $\lambda(z)$ on the transient ice-sheet evolution (*NH_λ*, Table 3-2), based on calculations for present-day Greenland ice sheet by Krinner and Genthon (1999) with slight adjustments according to Abe-Ouchi et al. (2007):

$if\ z \leq 1\,000\ m\ \lambda(z) = 4.3\ °C\,km^{-1}$

$if\ 1\,000\ m < z \leq 2\,000\ m\ \lambda(z) = 4.9\ °C\,km^{-1}$

$if\ 2\,000\ m < z \leq 3\,000\ m\ \lambda(z) = 6.1\ °C\,km^{-1}$

$if\ z > 3\,000\ m\ \lambda(z) = 7.9\ °C\,km^{-1}$

Second, we conduct a sensitivity simulation with another refreezing scheme for the Positive Degree Day (PDD) ablation model (*NH_PDD,* Table 3-2). In this simulation, the more complex refreezing scheme from Janssens and Huybrechts (2000), used in the reference simulation, is replaced by the basic refreezing model of Reeh (1991). In the Reeh (1991) model, it is assumed that 60 % of the melt water refreezes uniformly for every time step and grid point where surface melting occurs.

In summary, the sensitivity simulations with these SMB-related changes (*NH_λ* and *NH_PDD*) both result in slightly smaller ice sheets during the coldest period of the glacial cycle compared to *NH_CTL* (Figure 4-6a,b). As a result, the maximum ice volume in *NH_λ* and *NH_PDD* is about 15 m SLE lower than in *NH_CTL* (Table 4-1). This reduction in ice volume is mostly explained by a smaller North American ice sheet. The size of the Eurasian ice sheet also decreases as a result of changing the SMB parameterizations but to a lesser extent than the North American counterpart (Figure 4-6b).

4.1.4 Impact of sub-ice shelf melting and transient calving.

In this section, we analyse the sensitivity of the ice-sheet evolution to different values of the fixed thickness threshold for sub-ice shelf melting and calving. In addition, we modulate these processes during runtime based on an index derived from the global SST stack from Shakun et al. (2015) (referred to as S_{SHAKUN}). The SST stack is highly similar to that of $\delta^{18}O_{sw}$ used for the Shakun et al. (2015) climate index (Figure 3-1) but the SST evolution leads the $\delta^{18}O_{sw}$ signal for a few thousands of years and thus presents a slightly earlier timing of the maxima and minima compared with the climate index (see Figure 5b in Shakun et al. 2015).

The transient evolution for sub-ice shelf melting B_{melt} is defined as:

$B_{melt}(t) = b_{melt1} \times S_{SHAKUN} \qquad if\ z \geq 600\ m,$

$B_{melt}(t) = b_{melt2} \times S_{SHAKUN} \qquad if\ z < 600\ m,$

where b_{melt1} and b_{melt2} have prescribed values of 0.05 m a^{-1} and 0.6 m a^{-1} in order to account for the difference between the relatively cold surface and sub-surface ocean in the high latitudes and the deeper water masses from North Atlantic that are comparatively warmer. 600 m corresponds to the average depth of the continental shelf. In the other simulations presented in this study, when not specified otherwise, b_{melt1} and b_{melt2} are fixed at 0.1 m a^{-1} and 0.2 m a^{-1}, respectively, following the Colleoni et al. (2014a) and Quiquet et al. (2016).

The transient evolution of the thickness threshold for the calving front H_{coup} takes the following form:

$$H_{coup}\,(t) = H_{coup\_min} + \frac{H_{coup}}{2} \times S_{SHAKUN},$$

$$H_{coup}(t) = \max(H_{coup}(t), H_{coup\_min}),$$

$$H_{coup}(t) = \min(H_{coup}(t), H_{coup\_max}),$$

where H_{coup_min} and H_{coup_max} are set to 120 m and 180 m, respectively, so that when $S_{SHAKUN} = 1$, $H_{coup} = 200\ m$, which corresponds to the fixed prescribed value used in the previous studies (Colleoni et al. 2014a, Quiquet et al. 2016).

Allowing for a transient representation of the sub-ice shelf melting and calving (*NH_OCE*) generally results in a similar evolution of the Northern Hemisphere ice volume as in *NH_CTL* (Figure 4-6a). The only exception is a slight increase of the ice volume (~ 10 m SLE) with respect to *NH_CTL* between 140 and 160 ka BP, resulting from an increased size of the Eurasian ice sheet (Figure 4-6b). The larger Eurasian ice sheet in *NH_OCE* is primarily explained by a slightly earlier thickening of some of the marine-based sectors of the Eurasian ice sheet towards 160 ka compared to when using fixed values for the oceanic forcing.

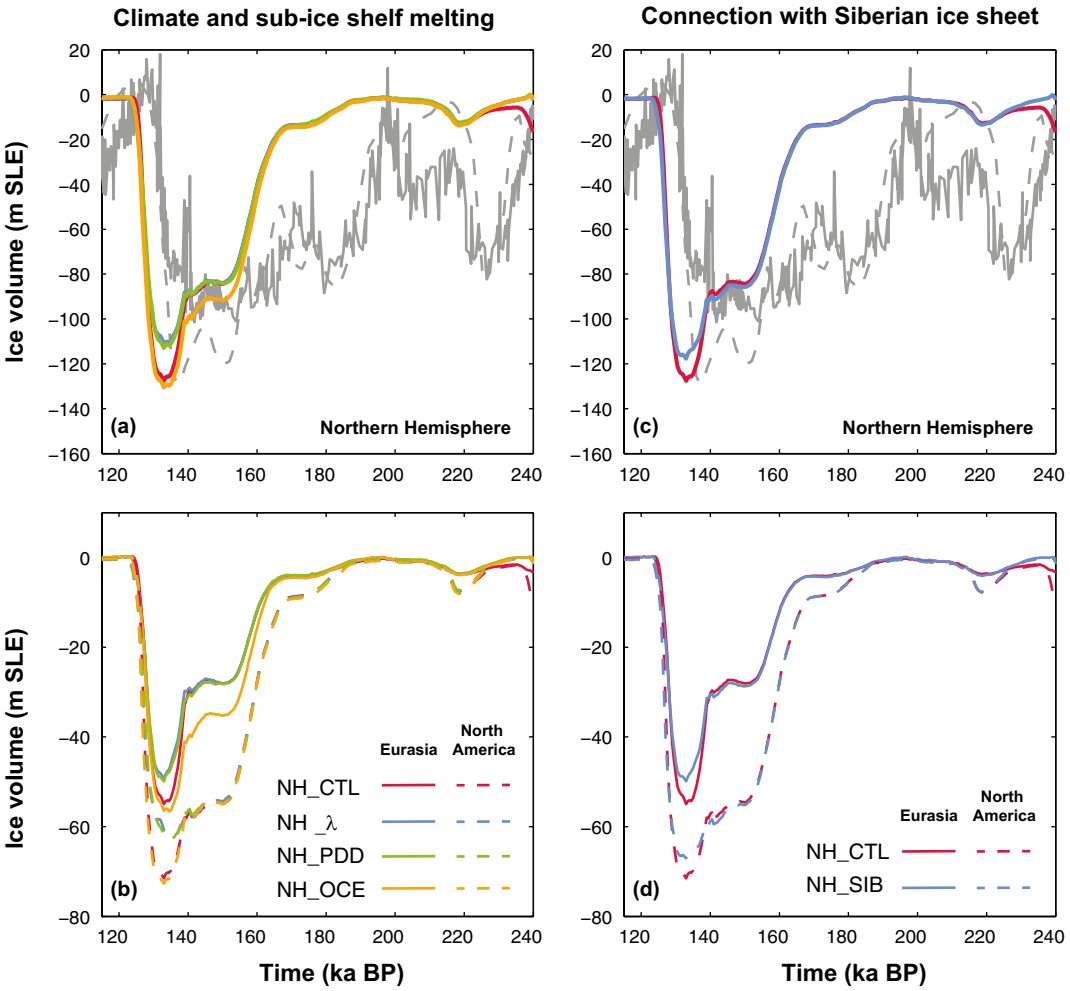

Figure 4-6. *Simulated transient ice volume (m SLE) in the control simulation (NH_CTL) together with the transient ice volume in the NH_λ, NH_PDD and NH_OCE and sensitivity simulations (Table 3-2) in panels (a) and (b), and the NH_SIB sensitivity simulation in panels (c) and (d). Panels (a) and (c) show the total simulated Northern Hemisphere ice volume, whereas panels (b) and (d) show the individual contributions from the Eurasian and North American ice sheets. Solid grey lines in panels (a) and (c) indicate the Red Sea relative sea level reconstruction from Grant et al. (2014), and dashed grey lines corresponds to deep-sea reconstructed sea level variations from Waelbroeck et al. (2002).*

4.1.5 Impact of the connection with the Siberian ice sheet

As discussed in Section 4.1, an ice sheet develops over Eastern Siberia in the transient simulations. In the control simulation and all other simulations presented thus far, we have, as previously described, imposed a heat corridor between the Siberian ice sheet and the adjacent Eurasian and North American ice sheets in order to disconnect them from one another (visible in e.g. Figure 4-2). Here we test the impact of this connection by removing the heat corridor and thereby allowing all ice sheets to be connected around the Arctic margins (Figure 4-7). The results show that the connection between the Siberian ice sheet and the adjacent ice sheets yields slightly thinner ice sheets during the glacial maximum, but it does not have any significant impact on the simulated ice volume for the reminder of the glacial cycle (Figure 4-6c,d, Table 4-1).

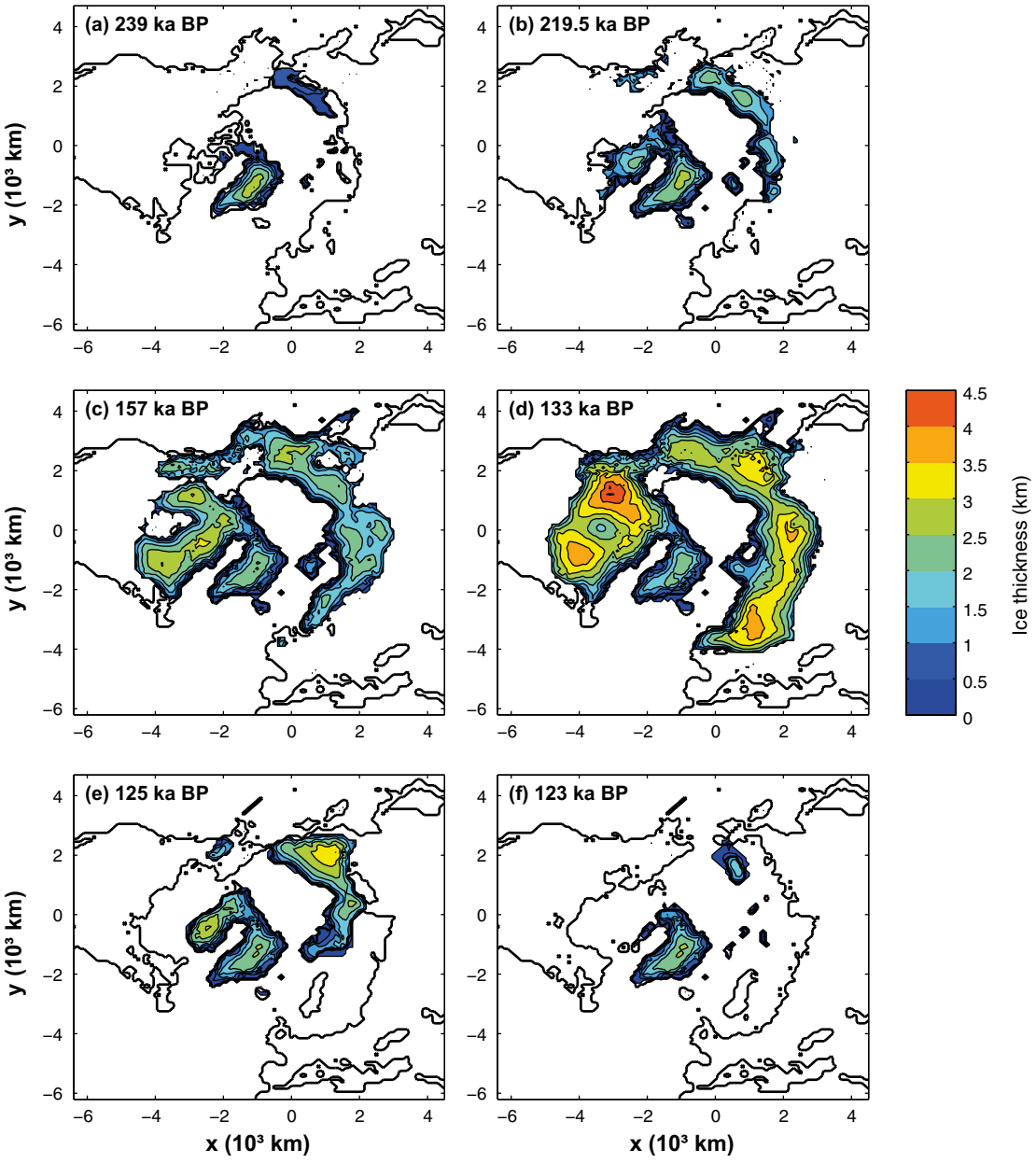

Figure 4-7. Simulated transient evolution of ice thickness when allowing connections between the Siberian ice sheet and the adjacent ice sheets (NH_SIB, Table 3-2).

4.2 Ice thickness at the Forsmark and Olkiluoto sites

In this section we present the evolution of the ice-sheet thickness over Forsmark and Olkiluoto based on the 100 km, as well as the 40 km, resolution simulations. In the control simulation with 100 km resolution (*NH_CTL*), glaciation of the Forsmark and Olkiluoto sites starts at about 160 ka BP (Figure 4-8). For the first ~ 20 ka after the initial glaciation the ice-sheet thickness over both sites is relatively modest, whereas it increases dramatically at around ~ 140 ka BP resulting in a maximum ice-sheet thickness of ~ 3 800 in the Forsmark area and 3 900 m in the Olkiluoto area (red lines in Figure 4-8, Table 4-1).

In *NH_BAR*, which uses the climate index based on Barker et al. (2011), the ice sheet thickness over Forsmark and Olkiluoto is significantly more variable than in *NH_CTL*. Whilst the total duration of glaciated conditions in *NH_BAR* is about three times that of *NH_CTL* (Figure 4-8), the resulting maximum ice thickness is about 500 m lower (Table 4-1). The use of Köhler et al. (2010) and Lisiecki and Raymo (2005) climate indices (*NH_KOH* and *NH_LIS*, respectively) does not allow the ice sheet to expand extensively over the Forsmark and Olkiluoto sites. Transient evolution of sub-ice shelf melting and calving (*NH_OCE*), elevation-dependent lapse rate (*NH_λ*) and the alternative refreezing scheme (*NH_PDD*) do not significantly influence the duration of the glaciation over Forsmark and Olkiluoto and result in a discrepancy in ice thickness of only some tens of meters compared to *NH_CTL* over both sites (Figure 4-8b,d, Table 4-1).

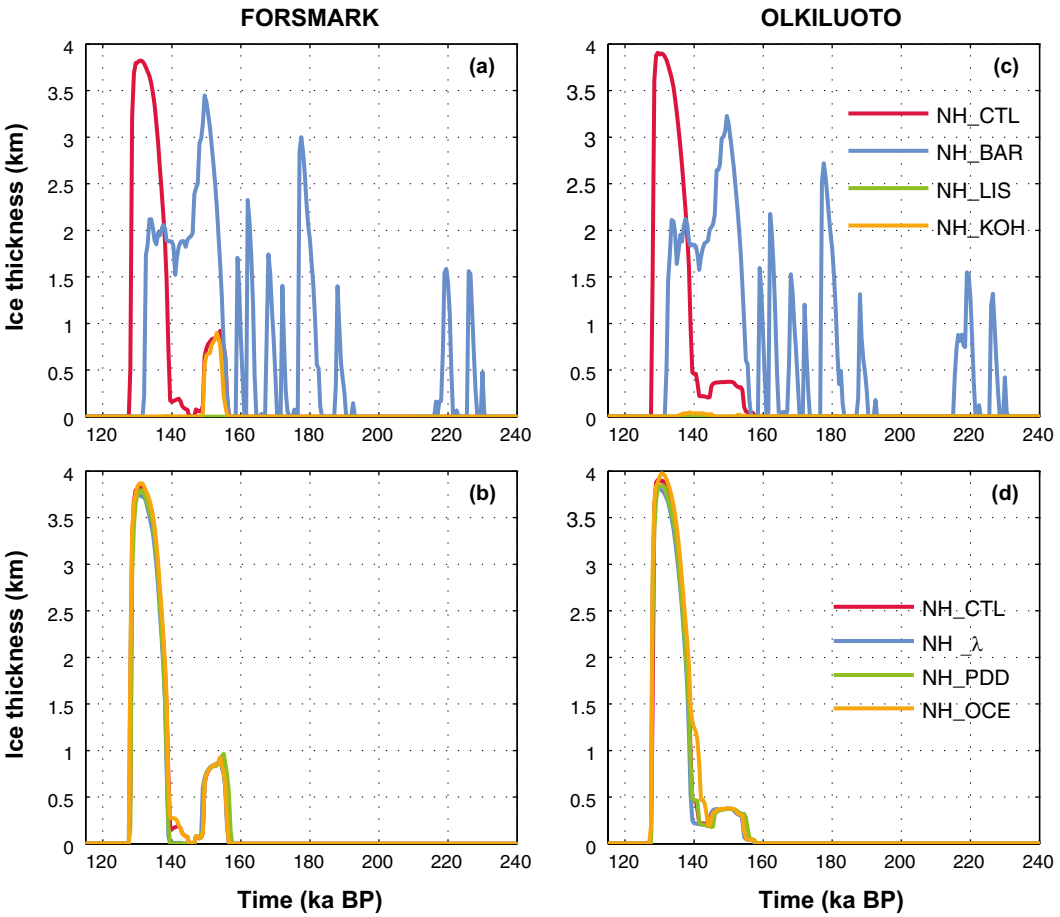

Figure 4-8. *Simulated transient evolution of ice thickness (m) over the Forsmark (a,b) and Olkiluoto (c,d) sites using 100 km horizontal resolution. Panels (a) and (c) show the ice thickness evolution in NH_CTL, NH_BAR, NH_KOH and NH_LIS, whereas panels (b) and (d) show the ice thickness evolution in NH_CTL, NH_λ, NH_OCE and NH_PDD.*

Using 40 km instead of 100 km horizontal resolution results in an increase of the maximum ice-sheet thickness by ~ 200 m at Forsmark and ~ 100 m at Olkiluoto (Table 4-1). To that end, using 40 km resolution, the ice-sheet thickness during the Saalian glacial maximum amounts to approximately 4 000 km over both repository sites. In general, however, the ice-sheet evolution in the control simulations with 40 km resolution (*NH40_CTL*) is very similar to corresponding simulation with 100 km (cf. Figure 4-2 and Figure 4-9). The difference in maximum ice volume between the simulations, occurring at 133 ka BP in both cases, is only about 2 m SLE (Table 4-1).

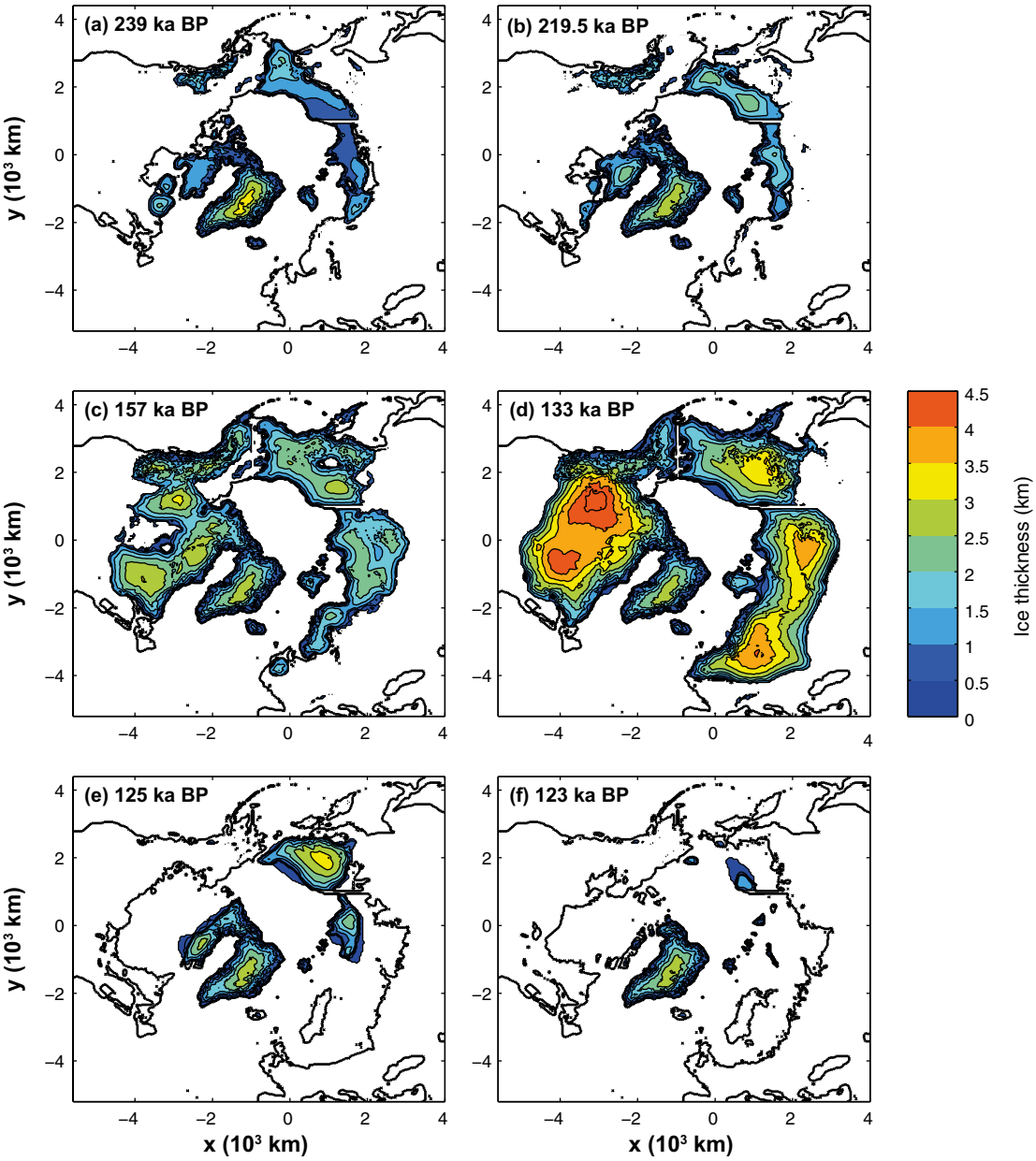

Figure 4-9. *Transient evolution of ice thickness (m) in the control simulation using 40 km resolution (NH40_CTL, see Table 3-2). Glacial maximum is reached at 133 ka BP.*

5 Discussion

In this section limitations and caveats of the methodology used in the present study are discussed.

5.1 Uncertainties related to climate snapshots and climate indices

First of all, we used climate snapshots that come from different versions and spatial resolutions of the same models, CESM 1.0.2 and CESM 1.0.5. It is well known that the CESM low resolution component has a cold bias in the Northern Hemisphere high latitudes because ocean heat transport is weak (see Colleoni et al. 2014b for further discussion about coupled climate model biases). In CESM 1.0.5, bottom water formation in the Southern Ocean does not occur at the correct locations, which induces biases in the inter-hemispheric ocean heat transport (Jochum et al. 2011, Shields et al. 2012). This model bias influences the atmospheric circulation which ultimately translates in the development of the Eastern Siberian ice sheet (Colleoni et al. 2016b), an ice sheet that is highly debated in the scientific literature (e.g. Stein et al. 2017). The use of a different climate model, able to reproduce planetary wave-induced temperature patterns in the Arctic region, might improve this aspect of the transient simulation. Furthermore, the interpolation between climate snapshots using climate indices is artificial and lacks representation of climate feedbacks that account for changes in e.g. the atmospheric/oceanic circulation, sea ice cover and vegetation cover that might also constrain the expansion or the retreat of the Northern Hemisphere ice sheets.

In the present study we used four different indices as representative for the temporal climate evolution. Our results show that the choice of climate index has a substantial impact on the Northern Hemisphere transient ice-sheet evolution. Most of the indices used in the present study are either not representative of the Northern Hemisphere climate evolution or they are artificially expanded over the Saalian glacial cycle (e.g. Barker et al. 2011). In addition, in the present study, we used a single curve as representative for climate development in the entire Northern Hemisphere which is not realistic. A way to improve this would be to find more suitable geological records to be applied separately to Eurasia and to North America. In fact, recent studies focusing on the last deglaciation have substantially improved the representation of the Eurasian deglaciation history by using regional index based on transient coupled climate simulations or different geological records for different macro-regions (Patton et al. 2016). However, unfortunately only few regional records exist for the Saalian glacial cycle and most of them do not have a sufficiently high temporal resolution. A poor temporal resolution would presumably influence the rate of expansion of the ice sheets in the numerical simulations.

5.2 Uncertainties related to parameters in the ice-sheet model

As described in Section 3.2, we used ice-sheet model parameter values representative for an “average case” of the Latin Hypercube ensemble in Quiquet et al. (2016), resulting in ~ 3 500 m steady-state Late Saalian ice sheet thickness at the repository sites. Here we explore the impact of using “extreme” parameter combinations from the Latin Hypercube ensemble, i.e. those that resulted in thicknesses greater than 4 000 m at the Forsmark and Olkiluoto sites, on the transient Saalian ice-sheet evolution. The parameter values used in this simulation is shown in Table 5-1 and the resulting evolution of the Northern Hemisphere ice volume is shown in Figure 5-1. Besides the different ice-sheet model parameter values presented in Table 5-1, the simulation with extreme parameters uses identical boundary conditions and climate forcing as in *NH_CTL*.

Using extreme parameters has a relatively minor impact on the Northern Hemisphere ice volume evolution compared to the simulation with average parameters, *NH_CTL* (Figure 5-1). Apart from a small increase of the Northern Hemisphere ice volume during the coldest period of the glacial cycle (between 130 and 160 ka BP), the simulation with extreme parameters is virtually identical to *NH_CTL*. The

maximum ice-sheet thickness in the Forsmark/Olkiluoto area in the simulations with extreme parameters is about 200 m greater than in *NH_CTL*, thus comparable with the ice-sheet thicknesses obtained when using average parameters and 40 km horizontal resolution (NH40_CTL, Table 4-1).

In summary, the evolution of the simulated ice volume and ice thickness appears to be significantly less sensitive to ice-sheet model parameters in the transient simulations presented here than in the steady-state simulations in Quiquet et al. (2016). Understanding this reduced sensitivity is beyond the scope of the present study. However, we anticipate that it is, at least to a certain extent, explained by the demonstrated strong ability of the climate indices to modulate the SMB and ensuing transient ice-sheet evolution. These indices are not included in steady-state simulations as these do not require a representation of the temporal climate variability.

Table 5-1. Ice-sheet model parameters values used in the simulation in the simulation resulting in the thickest ice sheets in Quiquet et al. (2016): λ is the atmospheric lapse rate (°C km^{-1}), γ the precipitation factor (‰), σ the amplitude of daily temperature cycle (°C), γ_{GHF} the geothermal heat flux modificator, C_{snow} the melting coefficient for snow (mm day^{-1} °C^{-1}), C_{ice} the melting coefficient for ice (mm day^{-1} °C^{-1}), P_{solid} the temperature threshold for snow (°C), d the thickness thickness of the thermo-active layer in the surface mass balance model, C_f the dragging coefficient, and EF the enhancement factor for SIA. The GHF modificator, γ_{GHF}, is multiplied with a baseline GHF distribution by Shapiro and Ritzwoller (2004) to obtain the actual GHF used in the model.

Parameter	Value
λ (°C km^{-1})	Annual: 4.6, Summer: 3.6
γ (°C^{-1})	0.047
σ (°C)	1.85
γ_{GHF}	1.11
C_{snow} (mm day^{-1} °C^{-1})	2.5
C_{ice} (mm day^{-1} °C^{-1})	7.4
P_{solid} (°C)	0.76
d (m)	0.65
C_f	9.27×10^{-5}
EF	1.96

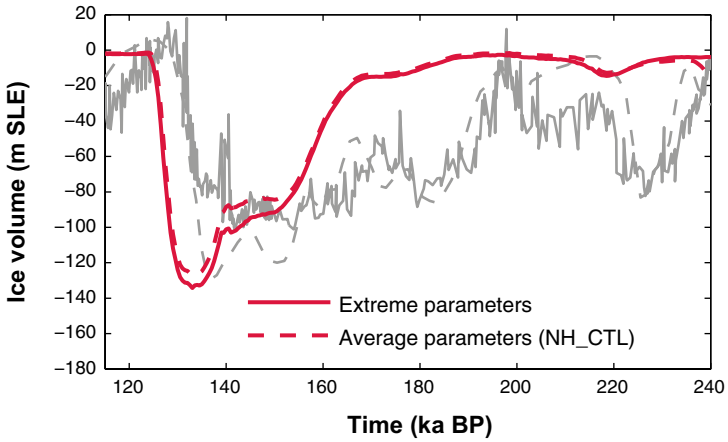

Figure 5-1. *Simulated transient Northern Hemisphere ice volume evolution (m SLE) using parameters that resulted in the thickest ice-sheets in Quiquet et al. (2016) ("extreme parameters", see Table 5-1; red solid line) and in the control simulation NH_CTL ("average parameters", see Table 3-3; red dashed line). The simulated Northern Hemisphere ice volume has been calculated with the Siberian ice sheet excluded. Grey solid and dashed curves correspond to Grant et al. (2014) and Waelbroeck et al. (2002) sea level reconstructions, respectively.*

5.3 Uncertanties related to the ice sheet configuration and volume during the Late Saalian glacial maximum

One of the main uncertainties is related to the actual extents and volumes of the ice sheets themselves. In a recent study, Rohling et al. (2017) attempted to understand how much the Eurasian ice sheet extent at the Late Saalian glacial maximum, at ~ 140 ka BP, differed from the reconstruction of the maximum Late Saalian extent in Svendsen et al. (2004). Based on a compilation of geological evidence, Rohling et al. (2017) suggested that while the ice sheet extent during the Late Saalian glacial maximum was smaller than the Eurasian ice-sheet extent used in the *CS140* climate snapshot, it was slightly larger than mid-Weichselian extent at ~ 60 ka BP (Figure 5-2). Similarly, there are very limited data on the extent of the North American ice sheet during the Saalian glacial cycle. The few existing geological observations show that Newfoundland was likely not covered by ice and that iceberg production was much lower than during the LGM (Hiscott et al. 2001, Naafs et al. 2013). Both sources of information indicate that the Late Saalian maximum North American ice sheet could have been smaller than during the LGM.

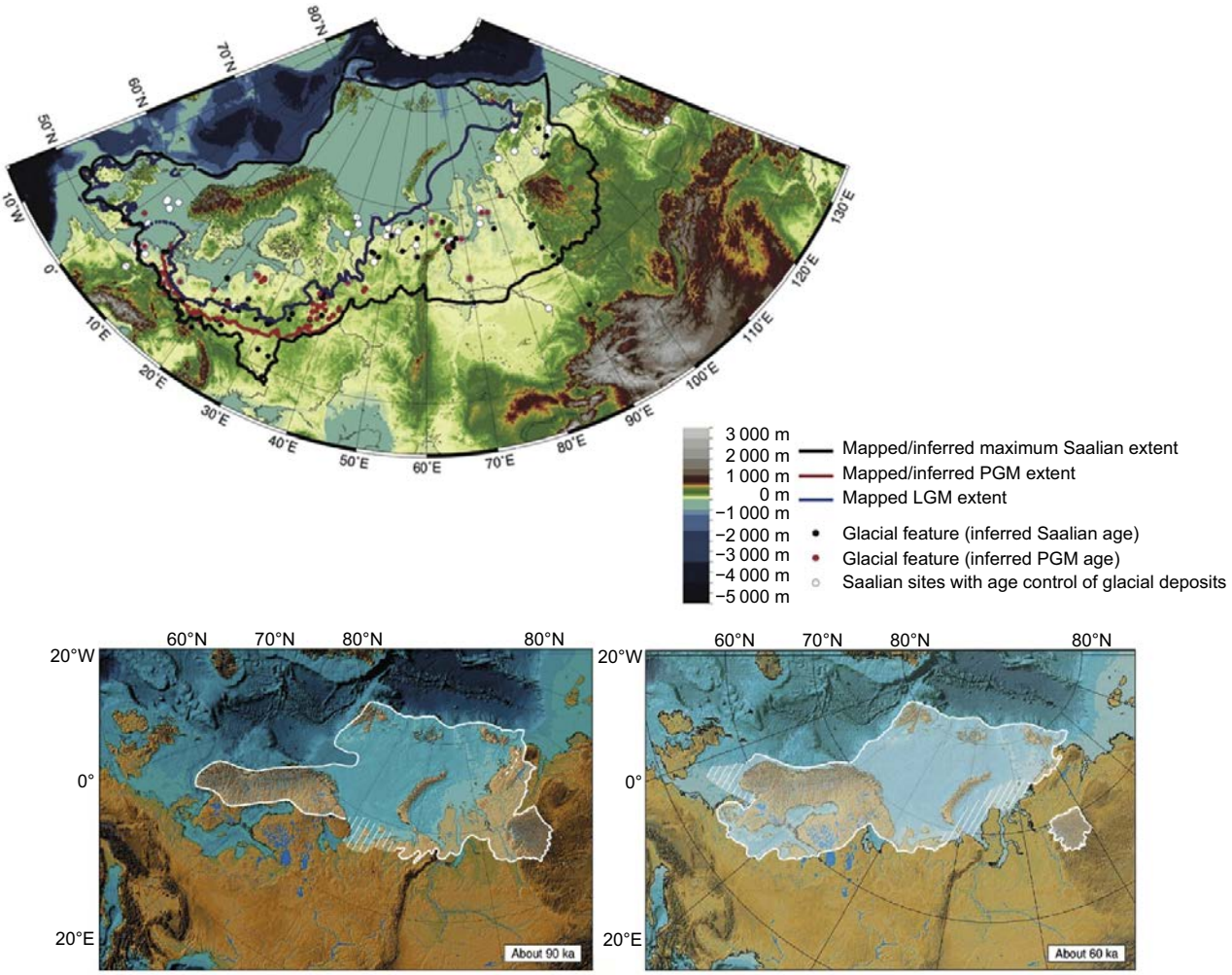

Figure 5-2. *Top: comparison of Eurasian ice sheet extent between Saalian glacial maximum (~ 140 ka BP) (reprinted from Rohling et al. 2017, Copyright 2017, with permission from Elsevier). Bottom: early (90 ka BP) and mid (60 ka BP) Weichselian (reprinted from Svendsen et al. 2004, Copyright 2004, with permission from Elsevier).*

Proxy reconstructions also suggest that the global sea level may have been higher by the Late Saalian glacial maximum than during the LGM (e.g. Rohling et al. 2017, Grant et al. 2014). Based on a comparison between different sea level reconstructions, Rohling et al. (2017) found that the difference between Late Saalian glacial maximum and LGM is in the order of 10 m SLE. The simulations carried out here present Northern Hemisphere ice volumes ranging from about 70 m SLE to 130 m SLE. Most of the simulations thus have Northern Hemisphere ice volumes that fall within the range of past sea level reconstructions. It is important to note that in all the simulations, from the middle of the Saalian glacial cycle, the North American ice sheet is larger than the Eurasian ice sheet in all simulations.

6 Conclusions

The objective of this study was to provide reasonable simulations of the transient evolution of the Eurasian ice sheet during the Saalian glacial cycle to be used as upper boundary condition (in terms of ice sheet thickness) in bedrock stress modelling. In the introduction we stated three conditions that should be fulfilled for a certain transient simulation to be regarded as a "reasonable":

i) The ice sheet build-up and decay should exhibit an ice-sheet evolution typical for the last 800 ka, i.e. a relatively slow build-up to a maximum ice-sheet extent followed by a rapid deglaciation.

ii) The simulated Northern Hemisphere ice volume during the Late Saalian glacial maximum should be in reasonable agreement with contemporary sea-level reconstructions of that time (~ 80–140 m lower than present-day).

iii) The ice sheet thickness over the repository sites Forsmark and Olkiluoto during the Late Saalian glacial maximum should be considerably greater than the Weichselian maximum ice sheet thickness, reconstructed by SKB to be ~ 2 900 m (e.g. SKB 2010).

In most of the simulations using the climate indices based on Shakun et al. (2015) and Barker et al. (2011), all three conditions are met. Using 100 km horizontal resolution, the simulated maximum ice thickness is ~ 3 800 – 3 900 m over the repository sites with the Shakun et al. (2015) climate index, and ~ 3 500 m and ~ 3 200 m over Forsmark and Olkiluoto, respectively, with the Barker et al. (2011) index. Using 40 km horizontal resolution, the maximum ice thickness reaches ~ 4 000 m over both sites, in agreement with the thickest ice sheets obtained from the steady-state ice sheet simualtions made by Colleoni et al. (2014a) and Quiquet et al. (2016). In the simulations using climate indices based on Köhler et al. (2010) and Lisiecki and Raymo (2005), the repository sites remain ice-free through the entire glacial cycle, thereby failing to meet condition (iii) above.

Although the simulations using the Shakun et al. (2015) and Barker et al. (2011) climate indices manage to fulfil the listed conditions, it is questionable if the geographical extents of the ice sheets in those simulations are realistic according to observational evidence. For example, in the Shakun et al. (2015) simulations, the simulated Northern Hemisphere ice volume is underestimated by up 70 m SLE compared with proxy data during the first part of the glacial cycle. Furthermore, the simulations in this study produce an ice sheet in Eastern Siberia whose existence is highly questionable. However, sensitivity simulations show that the existence of this ice sheet only has a minor influence on the evolution of the Eurasian ice sheet which is, ultimately, of primary importance in bedrock stress simulations. Therefore, we recommend that any simulations using the Shakun et al. (2015) and Barker et al. (2011) climate indices, in particular the simulation with the higher (40 km) spatial resolution, would be suitable to use as boundary condition when assessing the impact of extreme glaciation on the bedrock stress distribution in the Forsmark/Olkiluoto area.

References

SKB's (Svensk Kärnbränslehantering AB) publications can be found at www.skb.com/publications.

Abe-Ouchi A, Segawa T, Saito F, 2007. Climatic conditions for modelling the Northern Hemisphere ice sheets throughout the ice age cycle. Climate of the Past 3, 423–438.

Amante C, Eakins B W, 2009. ETOPO1 1 Arc-Minute Global Relief Model: procedures, data sources and analysis. NOAA Technical Memorandum NESDIS NGDC-24, National Geophysical Data Center, NOAA, Boulder, Colorado.

Barker S, Knorr G, Edwards R L, Parrenin F, Putnam A E, Skinner L C, Wolff E, Ziegler M, 2011. 800 000 years of abrupt climate variability. Science 334, 347–351.

Charbit S, Ritz C, Ramstein G, 2002. Simulations of Northern Hemisphere ice-sheet retreat:: sensitivity to physical mechanisms involved during the Last Deglaciation. Quaternary Science Reviews 21, 243–265.

Colleoni F, Wekerle C, Masina S, 2014a. Long-term safety of a planned geological repository for spent nuclear fuel in Forsmark – estimate of maximum ice sheet thicknesses. SKB TR-14-21, Svensk Kärnbränslehantering AB.

Colleoni F, Masina S, Cherchi A, Navarra A, Ritz C, Peyaud V, Otto-Bliesner B, 2014b. Modeling Northern Hemisphere ice-sheet distribution during MIS 5 and MIS 7 glacial inceptions. Climate of the Past 10, 269–291.

Colleoni F, Wekerle C, Näslund J O, Brandefelt J, Masina S, 2016a. Constraint on the penultimate glacial maximum Northern Hemisphere ice topography (~ 140 ka BP). Quaternary Science Reviews 137, 97–112.

Colleoni F, Kirchner N, Niessen F, Quiquet A, Liakka J, 2016b. An East Siberian ice shelf during the Late Pleistocene glaciations: Numerical reconstructions. Quaternary Science Reviews 147, 148–163.

Dendy S, Austermann J, Creveling J R, Mitrovica J X, 2017. Sensitivity of Last Interglacial sea-level high stands to ice sheet configuration during Marine Isotope Stage 6. Quaternary Science Reviews 171, 234–244.

Dutton A, Bard E, Antonioli F, Esat T M, Lambeck K, McCulloch M T, 2009. Phasing and amplitude of sea-level and climate change during the penultimate interglacial. Nature Geoscience 2, 355–359.

Dutton A, Carlson A E, Long A, Milne G A, Clark P U, DeConto R, Horton B P, Rahmstorf S, Raymo M E, 2015. Sea-level rise due to polar ice-sheet mass loss during past warm periods. Science 349. doi:10.1126/science.aaa4019

Dyke A S, Andrews J T, Clark P U, England J H, Miller G H, Shaw J, Veillette J J, 2002. The Laurentide and Innuitian ice sheets during the last glacial maximum. Quaternary Science Reviews 21, 9–31.

Gent P R, Danabasoglu G, Donner L J, Holland M M, Hunke E C, Jayne S R, Lawrence D M, Neale RB, Rasch P J, Vertenstein M, Worley P H, Yang Z-L, Zhang M, 2011. The Community Climate System Model Version 4. Journal of Climate 24, 4973–4991.

Grant K M, Rohling E J, Ramsey C B, Cheng H, Edwards R L, Florindo F, Heslop D, Marra F, Roberts P, Tamisiea M E, Williams F, 2014. Sea-level variability over five glacial cycles. Nature Communications 5, 5076. doi:10.1038/ncomms6076 (2014)

Hiscott R, Aksu A, Mudie P, Parsons D, 2001. A 340 000 year record of ice rafting, palaeoclimatic fluctuations, and shelf-crossing glacial advances in the south–western Labrador Sea. Global and Planetary Change 28, 227–240.

Janssens I, Huybrechts P, 2000. The treatment of meltwater retardation in mass-balance parameterizations of the Greenland ice sheet. Annals of Glaciology 31, 133–140.

Jochum M, Jahn A, Peacock S, Bailey D, Fasullo J, Kay J, Levis S, Otto-Bliesner B, 2011. True to Milankovitch: Glacial Inception in the new Community Climate System Model, Journal of Climate 25, 2226–2239.

Jouzel J, Masson-Delmotte V, Cattani O, Dreyfus G, Falourd S, Hoffmann G, Minster B, Nouet J, Barnola J M, Chappellaz J, Fischer H, Gallet J C, Johnsen S, Leuenberger M, Loulergue L, Luethi D, Oerter H, Parrenin F, Raisbeck G, Raynaud D, Schilt A, Schwander J, Selmo E, Souchez R, Spahni R, Stauffer B, Steffensen J, Stenni B, Stocker T F, Tison J L, Werner M, Wolff E W, 2007. Orbital and millennial Antarctic climate variability over the past 800 000 years. Science 317, 793–797.

Kleman J, Fastook J, Ebert K, Nilsson J, Caballero R, 2013. Pre-LGM Northern Hemisphere ice sheet topography. Climate of the Past 9, 2365–2378.

Köhler P, Bintanja R, Fischer H, Joos F, Knutti R, Lohmann G, Masson-Delmotte V, 2010. What caused Earth's temperature variations during the last 800 000 years? Data-based evidence on radiative forcing and constraints on climate sensitivity. Quaternary Science Reviews 29, 129–145.

Krinner G, Genthon C, 1999. Altitude dependence of the ice sheet surface climate. Geophysical Research Letters 26, 2227–2230.

Lagerbäck R, 1979. Neotectonic structures in northern Sweden. Geologiska Föreningens i Stockholm Förhandlingar 100, 263–269.

Liakka J, Löfverstrom M, 2018. Arctic warming induced by the Laurentide Ice Sheet topography. Climate of the Past 14, 887–900.

Liakka J, Löfverström M, Colleoni F, 2016. The impact of the North American glacial topography on the evolution of the Eurasian ice sheet over the last glacial cycle. Climate of the Past 12, 1225–1241.

Lisiecki L E, Raymo M E, 2005. A Pliocene–Pleistocene stack of 57 globally distributed benthic $\delta^{18}O$ records. Paleoceanography 20, PA1003. doi:10.1029/2004PA001071

Loulergue L, Schilt A, Spahni R, Masson-Delmotte V, Blunier T, Lemieux B, Barnola J-M, Raynaud D, Stocker T F, Chappellaz, J, 2008. Orbital and millennial-scale features of atmospheric CH_4 over the past 800 000 years. Nature 453, 383–386.

Lund B, Schmidt P, Hieronymus C, 2009. Stress evolution and fault stability during the Weichselian glacial cycle. SKB TR-09-15, Svensk Kärnbränslehantering AB.

Lüthi D, Le Floch M, Bereiter B, Blunier T, Barnola J M, Siegenthaler U, Raynaud D, Jouzel J, Fischer H, Kawamura K, Stocker T F, 2008. High-resolution carbon dioxide concentration record 650 000 – 800 000 years before present. Nature 453, 379–382.

Masson-Delmotte V, Stenni B, Pol K, Braconnot P, Cattani O, Falourd S, Kageyama M, Jouzel J, Landais A, Minster B, Barnola J M, Chappellaz J, Krinner G, Johnsen S, Röthlisberger R, Hansen J, Mikolajewicz U, Barnola J M, 2010. EPICA Dome C record of glacial and interglacial intensities. Quaternary Science Reviews 29, 113–128.

Naafs B, Hefter J, Stein R, 2013. Millennial-scale ice rafting events and Hudson Strait Heinrich (-like) events during the late Pliocene and Pleistocene: a review. Quaternary Science Reviews 80, 1–28.

Niessen F, Hong J K, Hegewald A, Matthiessen J, Stein R, Kim H, Kim S, Jensen L, Jokat W, Nam S-I, Kang S-H, 2013. Repeated Pleistocene glaciation of the East Siberian continental margin. Nature Geoscience 6, 842–846.

Patton H, Hubbard A, Andreassen K, Winsborrow M, Stroeven A P, 2016. The build-up, configuration, and dynamical sensitivity of the Eurasian ice-sheet complex to Late Weichselian climatic and oceanic forcing. Quaternary Science Reviews 153, 97–121.

Peltier W R, 2004. Global glacial isostacy and the surafce of the ice-age earth: The ICE-5G (VM2) model and GRACE. Annual Review of Earth and Planetary Sciences 32, 111–149.

Peyaud V, 2006. Role of the ice sheet dynamics in major climate changes. PhD thesis. Laboratoire de Glaciologie et de Géophysique de l'Environnement, Université Grenoble I.

Quiquet A, Colleoni F, Masina S, 2016. Long-term safety of a planned geological repository for spent nuclear fuel in Forsmark, Sweden and Olkiluoto, Finland. Phase 2: impact of ice sheet dynamics, climate forcing and multi-variate sensitivity analysis on maximum ice sheet thickness. SKB TR-16-02, Svensk Kärnbränslehantering AB.

Rabineau M, Berné S, Olivet J-L, Aslanian D, Guillocheau F, Joseph P, 2006. Paleo sea levels reconsidered from direct observation of paleoshoreline position during Glacial Maxima (for the last 500 000 yr). Earth and Planetary Science Letters 252, 119–137.

Reeh N, 1991. Parameterization of melt rate and surface temperature in the Greenland ice sheet. Polarforschung 59, 113–128.

Ritz C, Rommelaere V, Dumas C, 2001. Modeling the evolution of Antarctic ice sheet over the last 420 000 years: Implications for altitude changes in the Vostok region. Journal of Geophysical Research 106, 31943–31964.

Rohling E J, Hibbert F D, Williams F H, Grant K M, Marino G, Foster G L, Hennekam R, de Lange G J, Roberts A P, Yu J, Webster J M, Yokoyama Y, 2017. Differences between the last two glacial maxima and implications for ice-sheet, $\delta^{18}O$, and sea-level reconstructions. Quaternary Science Reviews 176, 1–28.

Shakun J D, Lea D W, Lisiecki L E, Raymo M E, 2015. An 800-kyr record of global surface ocean $\delta^{18}O$ and implications for ice volume-temperature coupling. Earth and Planetary Science Letters 426, 58–68.

Shapiro N M, Ritzwoller M H, 2004. Inferring surface heat flux distributions guided by a global seismic model: particular application to Antarctica. Earth and Planetary Science Letters 223, 213–224.

Shields C A, Bailey D A, Danabasoglu G, Jochum M, Kiehl J T, Levis S, Park S, 2012. The Low-Resolution CCSM4. Journal of Climate 25, 3993–4014.

Siddall M, Rohling E J, Almogi-Labin A, Hemleben C, Meischner D, Schmelzer I, Smeed D A, 2003. Sea-level fluctuations during the last glacial cycle. Nature 423, 853–858.

SKB, 2010. Climate and climate-related issues for the safety assessment SR-Site. SKB TR-10-49, Svensk Kärnbränslehantering AB.

SKB, 2011. Long-term safety for the final repository for spent nuclear fuel at Forsmark. Main report of the SR-Site project. SKB TR-11-01, Svensk Kärnbränslehantering AB.

Stein R, Fahl K, Gierz P, Niessen F, Lohmann G, 2017. Arctic Ocean sea ice cover during the penultimate glacial and the last interglacial. Nature Communications 8, 373. doi:10.1038/s41467-017-00552-1

Svendsen J I, Alexanderson H, Astakhov V I, Demidov I, Dowdeswell J A, Funder S, Gataullin V, Henriksen M, Hjort C, Houmark-Nielsen M, Hubberten H W, Ingólfsson Ó, Jakobsson M, Kjær K H, Larsen E, Lokrantz H, Lunkka J P, Lyså A, Mangerud J, Matiouchkov A, Murray A, Möller P, Niessen F, Nikolskaya O, Polyak L, Saarnisto M, Siegert C, Siegert M J, Spielhagen R F, Stein R, 2004. Late Quaternary ice sheet history of northern Eurasia. Quaternary Science Reviews 23, 1229–1271.

Tzedakis P C, Raynaud D, McManus J F, Berger A, Brovkin V, Kiefer T, 2009. Interglacial diversity. Nature Geoscience 2, 751–755.

Waelbroeck C, Labeyrie L, Michel E, Duplessy J C, McManus J F, Lambeck K, Balbon E, Labracherie M, 2002. Sea-level and deep water temperature changes derived from benthic foraminifera isotopic records. Quaternary Science Reviews 21, 295–305.

Arkitektkopia AB, Bromma, 2020

SKB is responsible for managing spent nuclear fuel and radioactive waste produced by the Swedish nuclear power plants such that man and the environment are protected in the near and distant future.

skb.se